공학박사 학위 논문

# Abnormal grain growth in metallic materials

## 금속 재료에서의 비정상 입자 성장

2016 년 8 월

서울대학교 대학원

재료공학부

심 형 석

# Abstract

## Abnormal grain growth in metallic materials

Hyung-Seok Shim

Department of Materials Science and Engineering

The Graduate School

Seoul National University

The mystery of selective abnormal grain growth of Goss oriented grain in Fe-3%Si steel has long remained unsolved since its discovery by Goss in 1933. Here, attempts to solve this puzzle are reviewed with a focus on sub-boundary enhanced solid-state wetting along the triple junction of polycrystalline metals. Especially, the grains with sub-boundaries of very low energy exclusively have a high probability to grow by solid-state wetting and as a result can grow abnormally. The microstructure at the initial stage of abnormal grain growth in Fe-3wt%Si steel was investigated using synchrotron X-ray microdiffraction to identify the sub-boundaries, which had been suggested to induce the selective AGG of Goss-oriented grains. The splitting of Laue diffraction peaks caused by sub-boundaries was observed only in Goss grains and not in matrix grains in the entire samples. The sub-boundaries were measured to have misorientation angles below 0.6° which is very low. The characteristics and morphologies of sub-boundaries in Goss grains were analyzed based on the splitting directions and positions of Laue diffraction peaks.

Based on the mechanism of sub-boundary enhanced solid state wetting and the

experimental results that shows the existence of sub-boundaries in abnormally growing Goss grains in Fe-3%Si steel, abnormal grain growth of non-Goss grains was induced by forming sub-boundary through low deformation in Fe-3%Si steel. The primary recrystallization specimens of Fe-3%Si was locally deformed by micro-indenter and annealed in order to form sub-boundary at matrix grains. After the specimens were subjected to secondary recrystallization, abnormal grain growth of non-Goss grains occurs. It was found that all of these abnormally grown grains which have totally different orientation with Goss grains had sub-boundary inside them. It is suggested that abnormal grain growth of grains which are desired to grow could be controlled and texture could made by forming sub-boundaries based on sub-boundary enhanced solid-state wetting mechanism.

The effect of an external electric field on recrystallization and grain growth during annealing was investigated in pure iron and Fe-2.9%Si alloy. The elimination behavior of island grains inside abnormally grown grains by the external electric field was also investigated in Fe-3%Si steel and Al 5052 alloy. It was observed that recrystallization, grain growth and the elimination of island grains were accelerated when the external electric field was applied during annealing. It is suggested that the crystal defects and nearby atoms could easily overcome the activation energies for the recrystallization and the grain boundary migration because the excess electric charges at surface of metal induced by the external electric field could excite the energy state of the crystal defects and nearby atoms.

---

**Keywords**: Abnormal grain growth; solid-state wetting; sub-boundary; synchrotron X-ray microdiffraction; electric field; recrystallization; grain growth.

***Student Number***: 2011-20648

# Contents

# List of figures

**Fig. 2.2.** The experimental configuration of synchrotron X-ray microdiffraction in 4B beamline at PAL. (a) The schematic (b) the real configuration

**Fig. 2.3.** (a) Schematic of crystal which has a sub-boundary. (b) Shape of Laue diffraction peaks between the area without (I) and with (II) sub-boundary.

**Fig. 2.4.** (a) Microstructures of Goss grains at the initial stage of AGG. (b) Splitting of (011) Laue diffraction peaks in $\theta$-$\chi$ space at four locations (A, B, C and D) in abnormally growing Goss grains.

**Fig. 2.5.** Intensity profiles along the direction $\xi$ at four locations (A, B, C and D) in abnormally growing Goss grains.

**Fig. 2.6.** Distribution of sub-boundaries in abnormally growing Goss grains expressed by marking positions where splitting of Laue peaks occurs.

**Fig. 3.1.** The possibility for the abnormal grain growth of non-Goss grain by formation of sub-boundary.

**Fig. 3.2.** The microstructure of macro-etched specimens after annealing. (a) 3 kgf, (b) 6 kgf, (c) 12 kgf and (d) 18 kgf.

**Fig. 3.3.** Orientation map analyzed by Synchrotron X-ray microdiffraction. (a) 3 kgf, (b) 6 kgf, (c) 12 kgf and (d) 18 kgf

**Fig. 3.4.** Splitting of $(\bar{1}\,\bar{1}\,4)$ Laue diffraction peaks in θ-χ space and intensity profiles along the direction ξ at specific locations in abnormally growing grains induced by indentation under the load of 3 kgf.

**Fig. 3.5.** Splitting of $(\bar{1}\,\bar{2}\,3)$ Laue diffraction peaks in θ-χ space and intensity profiles along the direction ξ at specific locations in abnormally growing grains induced by indentation under the load of 6 kgf.

**Fig. 3.6.** Splitting of Laue diffraction peaks in θ-χ space at specific locations in abnormally growing grains induced by indentation under the load of 12 kgf.

**Fig. 3.7.** Intensity profiles along the splitting direction of Laue diffraction peaks in Fig 3.6 at specific locations in abnormally growing grains induced by indentation under the load of 12 kgf.

**Fig. 3.8.** Splitting of Laue diffraction peaks in θ-χ space at specific locations in abnormally growing grains induced by indentation under the load of 18 kgf.

**Fig. 3.9.** Intensity profiles along the splitting direction of Laue diffraction peaks in Fig 3.8 at specific locations in abnormally growing grains induced by indentation

under the load of 18 kgf.

**Fig. 4.1.** The experimental configuration for annealing with and without the external electric field.

**Fig. 4.2.** The microstructures of pure iron specimens annealed without the external electric field at (a) 500 °C, (b) 600 °C, (c) 700 °C and (d) 800 °C.

**Fig. 4.3.** The microstructures of pure iron specimens annealed with the external electric field of 4 kV/cm at (a) 500 °C, (b) 600 °C, (c) 700 °C and (d) 800 °C.

**Fig. 4.4.** The microstructures of Fe-2.9%Si alloy specimens annealed without the external electric field at (a) 650 °C, (b) 700 °C, (c) 750 °C and (d) 800 °C.

**Fig. 4.5.** The microstructures of Fe-2.9%Si alloy specimens annealed with the external electric field of 4 kV/cm at (a) 650 °C, (b) 700 °C, (c) 750 °C and (d) 800 °C.

**Fig. 4.6.** The Vickers hardness of specimens after annealing with and without the external electric field of 4 kV/cm in (a) pure iron and (b) Fe-2.9%Si alloy.

**Fig. 4.7.** Microstructures of pure iron specimens after (a) recrystallization (annealed at 800 °C for 20 sec), (b) annealing at 800 °C 40 sec without the external electric field and (c) annealing at 800 °C 40 sec with the external electric field of 4 kV/cm.

**Fig. 4.8.** Microstructures of Fe-2.9%Si alloy specimens after (a) recrystallization (annealed at 900 °C for 30 sec), (b) annealing at 900 °C 150 sec without the external electric field and (c) annealing at 900 °C 150 sec with the external electric field of 4 kV/cm.

**Fig. 4.9.** (a) IPF map of specimens of Fe-3%Si steel at initial state ( specimen heated up to 1100 °C at 5 °C/min and held 30 min) (b) IPF map after filtering grains except the island grains.

**Fig. 4.10.** IPF map of specimens which annealed for 5 h and 10 h at 1100 °C with and without the external electric field.

**Fig. 4.11.** IPF map of specimens which annealed for 5 h and 10 h at 1100 °C with and without the external electric field after filtering grains except island grains.

**Fig. 4.12.** IPF map of specimens of Al 5052 alloy at initial state (specimens annealed at 530 °C for 2h) for annealing (a) without the external electric field (b) with the external electric field of 2.8 kV/cm.

**Fig. 4.13.** IPF map of specimens which annealed for 5 h and 10 h at 570 °C with and without the external electric field after filtering grains except island grains.

# List of tables

# Part 1. Abnormal grain growth in metallic materials approached by sub-boundary enhanced solid state wetting

# Chapter 1. Introduction: Abnormal Grain growth in metallic materials

## 1.1 Abnormal grain growth in metallic materials

The type of grain growth can be divided into two categories: normal grain growth (NGG) and abnormal grain growth (AGG) [1]. The grain size increases gradually and homogenously during NGG and the grain size distribution normalized by the average size does not change with annealing time. The grain growth decreases the area of the grain boundary lowering the total grain boundary energy. During AGG, On the other hand, only a few grains grow exclusively consuming the neighboring matrix grains, which shows a transient bimodal grain size distribution consisting of large abnormally grown grains and small matrix grains before impingements among abnormally grown grains. AGG which is also called discontinuous grain growth or secondary recrystallization normally occurs when NGG is inhibited by finely dispersed precipitates or a strong texture.

AGG takes place in many metallic materials especially after heat treatment of deformed polycrystalline metals. AGG was reported in copper-based alloy [2],

zirconium-based alloy [3, 4], ferritic stainless steel [5, 6], nickel-based alloy [7-9] and aluminum alloys [10-15]. AGG was also reported in pure metal [16-20], which indicate that precipitates are not essential to AGG. Furthermore, AGG also occurs not only in bulk metals but also in metallic films such as silver thin films [21, 22], copper thin films [23-25] and electro-deposited nickel films [26-28] during annealing. In general, it is known that AGG in bulk materials is harmful because AGG significantly degrades mechanical properties. AGG is also harmful in nanostructured materials because it changes the nanostructure instantly into a coarse structure of micron size [29, 30].

Fe-3%Si steel is the most famous alloy among the various metallic materials showing AGG. The Fe-3%Si steel has been studied more intensively than other systems mainly for two reasons. One is that AGG in Fe-3%Si steel is unusual in that the grains of so-called Goss orientation {110}<001> selectively undergo AGG (Fig. 1.1) and as a result a strong Goss texture is evolved after secondary recrystallization (Fig. 1.2). The other is that the strong Goss texture after AGG in Fe-3%Si steel has a beneficial effect on the magnetic properties. Because the <001> crystal direction is the easiest direction of magnetization in iron [31], the sharp Goss texture shows excellent magnetic properties such as low core loss and high permeability along the rolling direction. So Fe-3%Si steel is produced to undergo extensive AGG for application for the core material in transformers [32]. The sharpness of Goss texture, especially the deviation angle of <001> axis from the rolling direction, is closely related to its magnetic properties [33]. Thus, it is important to understand the mechanism of AGG and control sharp Goss texture. However, the mechanism of AGG is not yet clearly understood. The selective AGG of Goss grains may be one

of the most famous puzzles that have remained unsolved in metallic materials.

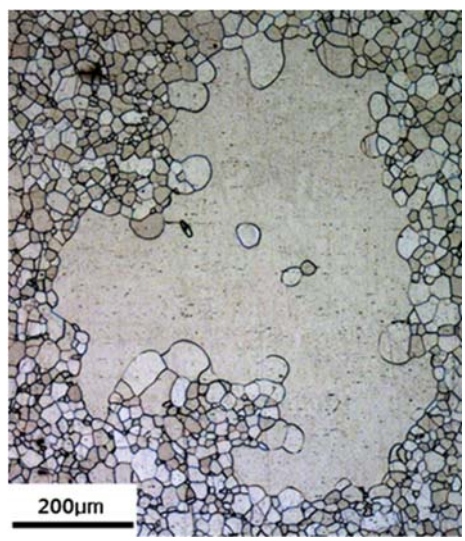


**Fig. 1.1.** Typical microstructure in the initial stage of secondary recrystallization of Fe-3%Si steel. An abnormally growing Goss grain has many island and peninsular grains.

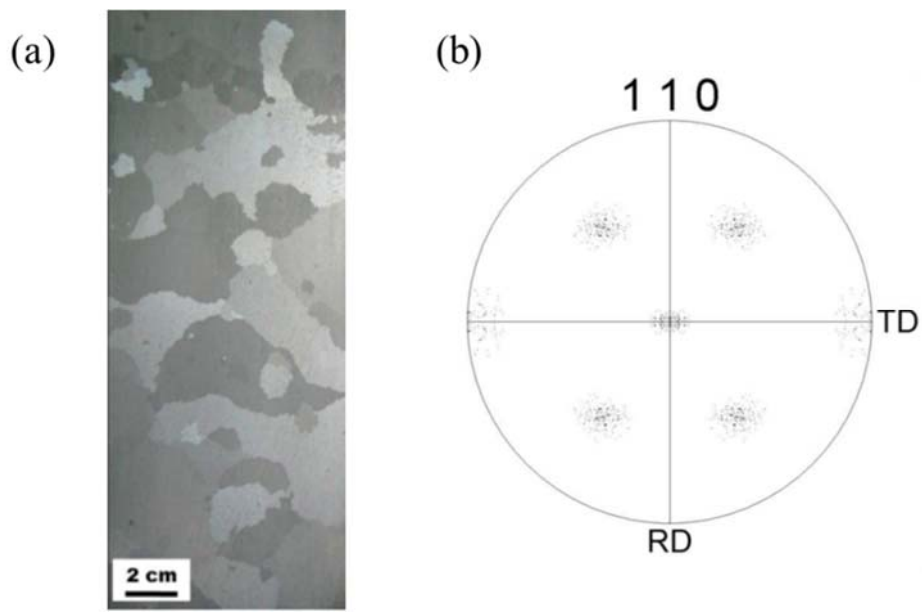


**Fig. 1.2.** (a) Microstructure of commercially produced Fe-3%Si steel after secondary recrystallization and (b) its pole figure of <110> direction obtained by X-ray diffraction.

## 1.2 Mechanisms suggested as selected AGG of Goss grains in Fe-3%Si steel

In Fe-3%Si steel, there is a puzzle as to why grains having Goss orientation selectively undergo AGG. Extensive efforts have been made to understand the selective AGG of Goss grains since its first report by Goss in 1935 [34]. However, this 80-year-old puzzle has not yet been solved so far. A lot of suggestion have been made as the mechanism of the selective AGG of Goss-oriented grains since 1935.

It was suggested at first that the initial size advantage of Goss grains over other matrix grains after primary recrystallization should be responsible for selective AGG of Goss grains. May and Turnbull [35] suggested that Goss grains might have larger grain size than other matrix grains after primary recrystallization and this size advantage gives a larger driving force for growth, which helps in unpinning of Goss grains from finely dispersed precipitates. Similarly, Hillert [1] and Rios [36-38] also suggested that a large grain can grow abnormally because the size advantage provides a large driving force which can overcome the Zener pinning force of precipitates. According to this suggestion, the grain size of Goss grains after primary recrystallization should be larger than that of matrix grains. However, Pease et al. [39], Lin et al. [40] and Chen et al. [41] reported that the size advantage cannot explain AGG because they confirmed that the size of Goss grains was not particularly larger than the average size of other grains when they observed the microstructure after primary recrystallization. Later, the observation that the Goss grains were not exclusively larger than the other matrix grains was reproducibly made.

In the meanwhile, the technique to determine the crystallographic orientation of grains, which is known as electron backscattered diffraction (EBSD), was developed in 1980s. Inokuti et al. [42] and Harase et al. [43, 44] actively utilized this EBSD technique for misorientation measurements in studying the mechanism of selective Goss AGG.

Inokuti et al. [42] suggested a geometrical coalescence model as a mechanism of selective Goss AGG based on their experimental observation with annealing time and the determination of Goss orientation. In the initial stage, they observed that Goss nuclei were independently formed and grown near the steel surface, whose location corresponded to Goss areas having been formed by hot rolling. Then, these primary Goss nuclei underwent the coalescence into one large Goss grain and this large Goss grain grows abnormally and the pancake shaped secondary Goss grain is finally evolved. The geometrical coalescence model is meaningful in that it is based on experimental observation. However, they could not explain how Goss nuclei are formed. Neither, could they explain how the independently-formed Goss nuclei coalescence into a single Goss grain.

Harase et al. [43, 44] and Shimizu et al. [45] suggested that coincidence site lattice (CSL) boundaries, especially Σ9 boundary, play a key role for Goss grain to undergo AGG. They investigated the misorientation relationship between Goss grains and other matrix grains in primary recrystallized microstructure and reported that Goss grains have a high percentage of CSL or Σ9 orientation relationship with matrix grains after primary recrystallization. Based on the assumption that the CSL and Σ9 boundaries should have a higher mobility than general grain boundaries, they suggested that Goss grains undergo AGG, consuming neighboring matrix grains

having CSL or Σ9 relationship [43, 44]. Yoshitomi et al. [46, 47] and Lin et al. [40] also reported that Goss grains have a high frequency of low CSL relationship such as Σ3, Σ5 and Σ7 with matrix grains after primary recrystallization and suggested that selective AGG of Goss grains is caused by high mobility of these CSL boundaries.

In contrast to this approach based on the high mobility of CSL grain boundaries, Ushigami et al. [48-52], Kumano et al. [53, 54], Homma et al. [55, 56] and Hutchinson [57] suggested that Goss grains have a high fraction of Σ9 boundaries which have low energy and thereby can overcome the pinning force of precipitates with ease and that Σ9 boundaries are responsible for selective Goss AGG. Maazi and Penelle [58] also suggested that CSL boundaries, which have low energy and can easily overcome the pinning force of precipitates, are responsible for the selective Goss AGG using computer simulation. They tried to show this possibility by Monte Carlo simulation considering a real microstructure in primary recrystallization and an effect of pinning force through setting a critical radius of neighbor grains to overcome the Zener force. They reported that simulation result reproduced the real microstructure of the initial stage in secondary recrystallization when Σ9 boundaries between Goss and matrix grains are assumed to have the low pinning force. So they considered that the selective AGG of Goss grains is closely related with the high percentage of CSL boundaries.

However, these suggestions based on CSL grain boundaries were criticized by Rajmohan et al. [59-61] and Hayakawa et al. [62-65] . They reported that the grain boundaries, of which Goss grains have the highest fraction, are not CSL grain boundaries but high-angle boundaries with misorientations in the range of 20-45°.

In agreement with these reports, Park et al. [66] made extensive EBSD measurements and confirmed that Goss grains have the highest fraction of high-angle grain boundaries instead of CSL grain boundaries. Based on the experimental observation that Goss grains have the highest fraction of high-angle boundaries, Hayakawa and Szpunar [63, 64] tried to explain the selective AGG of Goss grains by suggesting that the high-angle boundaries in the range of 20-45° are highly mobile because of their open structure, which provide the high diffusion path, resulting in rapid coarsening of precipitates, which weakens the pinning force during secondary recrystallization. However, Harase et al. [67] contradicted their explanation by reporting that some of grains which are not Goss orientation also have a high fraction of high-angle grain boundaries with misorientations in the range of 20-45° after primary recrystallization.

On the other hand, Etter et al. [68, 69] analyzed misorientation relationship between Goss grain and matrix grains after primary recrystallization extensively and concluded that both theories based on CSL and high angle grain boundaries could not properly explain the selective AGG of Goss grains. They measured that the percentage of CSL boundaries (Σ1~ Σ29b) around Goss gains is 17% which is the same as that in the primary matrix. They also found that the percentage of Σ9 boundary surrounding the Goss grain is only 0.3% which is lower than that in matrix grains, which is about 3%, and reported that the Goss grain didn't have a higher percentage of CSL relationship with matrix grains than other-oriented grains. Additionally, they investigated the misorientation relationship with the Goss grain of disappearing and remaining matrix grains during secondary recrystallization and reported that high-angle boundaries in the range of 20-45° have the highest

percentage of not only disappearing grains but also remaining grains during secondary recrystallization. This means that high-angle boundaries do not have a mobility advantage. Similarly, Morawiec [70] reported that it is not sufficient to explain the growth advantage of the Goss grain using only misorientations of grain boundaries because non-Goss grains in primary matrix grains also have the high fraction of CSL grain boundaries, especially Σ9 boundary, and 20-45° high angle grain boundaries like Goss grains.

Dorner et al. [71] tried to trace the Goss grains during cold rolling, primary recrystallization and secondary recrystallization using the Goss single crystal as starting material. Since they started from the Goss single crystal, an appreciable amount of Goss grains survived after primary recrystallization. By examining the microstructure after primary recrystallization, they found out a unique feature of Goss grains: only Goss grains have very small-angle grain boundaries with misorientation less than 1°. Based on this observation, they suggested that sub-boundaries in Goss grains provide the high diffusion path to dissolve precipitates and as a result Goss grains with sub-boundaries are less affected by the pinning force of precipitates, resulting in selective AGG of Goss grains. Their suggestion as to the role of sub-boundaries in Goss grains is not convincing because sub-boundaries consisting of dislocation arrays cannot provide a higher diffusion path than high angle boundaries.

## 1.3 Solid state wetting

The migration of grain boundary is driven by the grain boundary curvature in polycrystalline materials. The direction of the grain boundary migration is determined by the grain boundary curvature, which is a consequence of the force balance at the triple junction. If a grain has an inward grain boundary curvature, the grain grows in the direction to flatten the curvature. If a grain has an outward curvature, the grain shrinks in the direction to flatten the curvature. Fig. 1.3 shows a two dimensional schematic of shrinking 'A' and growing 'C' grains in contact with each other. It should be noted that the triple junction and the grain boundary appear, respectively, as the point and the line on the two-dimensional section. The maximum limit of the grain boundary migration is designated as the straight dashed line in Fig. 1.3 In this case, the grain boundary curvature disappears and there exists no driving force for further grain boundary migration. In other words, the grain boundary cannot migrate ahead of its triple junction even if the grain boundary has extremely high mobility.

Gottstein et al. [72-74] observed that the triple junction migration is generally slower than the grain boundary migration, becoming a rate-determining step in grain growth. Based on these observations, they suggested that the grain boundary migration is controlled by the migration of triple junctions in a three-dimensional polycrystalline structure. In this sense, the migration of grain boundaries is not independent but is kinetically coupled with the migration of triple junctions. In other words, the migration of grain boundaries is controlled by the migration of triple junctions.

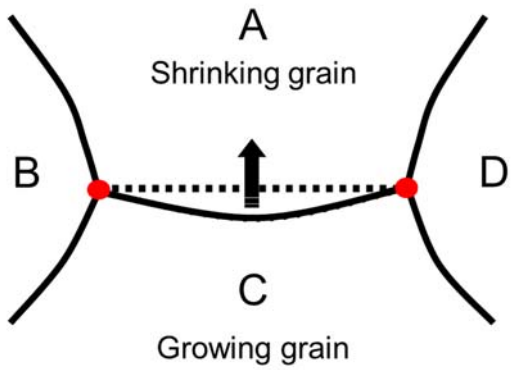


**Fig. 1.3.** Schematic showing the relation between the triple junctions and the grain boundary for grains A, B, C and D. Grains A and C are shrinking and growing, respectively, as indicated by the arrow and the grain boundary curvature.

However, it is experimentally evident that the grain boundaries of abnormally-growing grains migrate with extremely high rates. Considering the kinetic coupling between the grain boundary and the triple junction, in order for AGG to occur, there must be some mechanism by which the constraint imposed by triple junctions disappears. Regarding this aspect as the key point to understand the AGG, Hwang et al. [75-77] tried to find out the condition under which the constraint imposed by the triple junction disappears. They found out that the kinetic coupling between the grain boundary and the triple junction disappears when solid-state wetting and thereby the constraint disappears.

Fig. 1.4 shows schematics of solid state wetting mechanism. $\gamma_{AB}$, $\gamma_{BC}$ and $\gamma_{CA}$ represent the energy of grain boundaries between grains of subscript. In the solid state wetting along the grain boundary illustrated in Fig. 1.4, the grain A wets or penetrates the grain boundary between the grains B and C when the condition that $\gamma_{BC}$ is higher than the sum of $\gamma_{AB}$ and $\gamma_{AC}$ was satisfied.

$$\gamma_{BC} > \gamma_{AB} + \gamma_{AC} \quad (1)$$

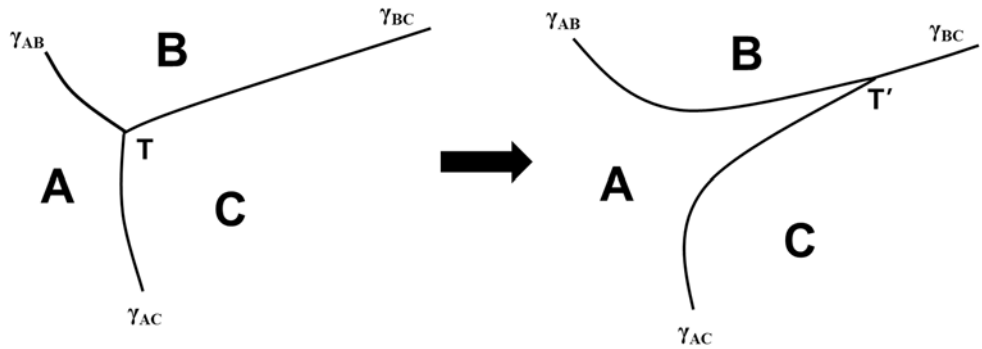


**Fig. 1.4.** Schematics illustrating solid-state wetting where a high energy grain boundary is penetrated by two low energy boundaries.

As the grain A penetrates the grain boundary in Fig. 1.4, the triple junction migrates from T to T' much faster than the grain boundaries between the grains A and B and between the grains A and C [78]. Therefore, the triple junction does not impose any constraint on the migration of the grain boundaries shared by the grain A with the grains B and C. Being free from the constraint, the boundaries of the grain A can migrate sufficiently fast for AGG. Therefore, if the grain A can continue to grow by solid-state wetting, it can grow abnormally. According to Hwang et al. [76], in a three-dimensional polycrystalline structure, the solid state wetting occurs along the triple junction line starting at a quadruple point because the energetic condition for triple-junction wetting is much easier to be satisfied than that for grain boundary wetting. The energetic condition of solid-state wetting along the triple junction line

can be expressed in terms of the grain boundary energy of 6 grain boundaries instead of the dihedral angle as follows [79].

$$\gamma_{BC} + \gamma_{CD} + \gamma_{BD} \geq \sqrt{3}\left(\gamma_{AB} + \gamma_{AC} + \gamma_{AD}\right) \tag{2}$$

Here, γ is the grain boundary energy between the two grains indicated by the subscripts.

## 1.4 Sub-boundary enhanced solid-state wetting

Considering Hwang et al.'s suggestion that AGG occurs by solid-state wetting, then why only Goss grains selectively grow abnormally in Fe-3%Si steel? Park et al. [66] suggested that Goss grains selectively have sub-boundaries of extremely low energy and proposed sub-boundary enhanced solid-state wetting mechanism.

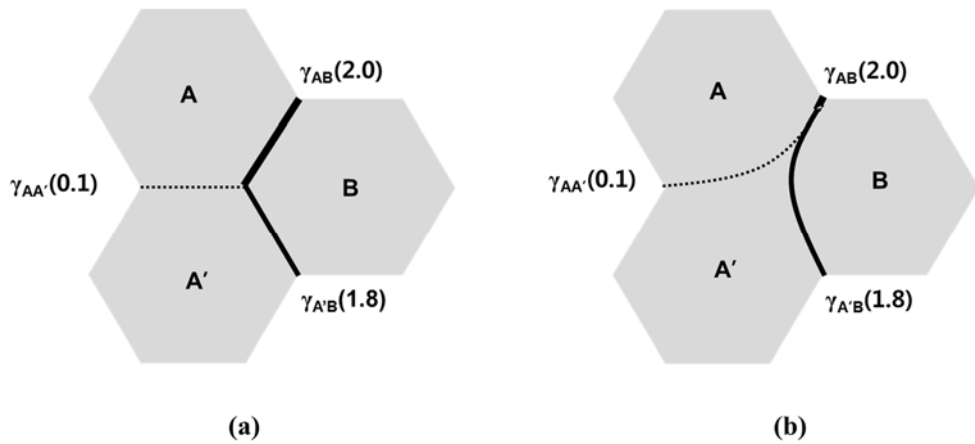


**Fig. 1.5.** Schematics showing how the sub-boundary of low energy can increase the probability of solid-state wetting.

Park et al. [66] suggested that the selective AGG of Goss grains can be satisfactorily explained by sub-boundary enhanced solid-state wetting because sub-boundaries drastically increase the probability of wetting. Fig. 1.5 shows how the sub-boundary increases the probability of solid-state wetting. Consider the three grains, A, A' and B in contact. Let us assume that grains A and A' share the sub-boundary with its energy of 0.1. Let us also assume that in Fig. 1.5(a) grains A and B have a boundary with energy of 2.0 and grains A' and C have a boundary with energy of 1.8. Since

$0.1 + 1.8 < 2.0$, the grain boundary between grains A and B is penetrated by the grain A' or replaced by the grain boundaries between grains A and A' and between grains A' and B as shown in Fig. 1.5(b). Since the grains A and A' share the low-energy boundary of $\gamma_{AA'} = 0.1$, either of them can grow by wetting the grain boundaries made with the third grain B if the difference between $\gamma_{AB}$ and $\gamma_{A'B}$ is larger than $\gamma_{AA'} = 0.1$. Therefore, grains A and A' sharing the sub-boundary of very low energy cooperate with each other to grow by solid-state wetting. In other words, the presence of sub-boundaries markedly increases the probability of wetting. Although Fig. 1.5 illustrates the case of grain boundary wetting for ease understanding, triple-junction wetting occurs actually in a three-dimensional polycrystalline structure for a given anisotropic grain boundary energy [76].

The possibility that the presence of sub-boundaries should induce the selective AGG was examined by computer simulation of grain growth. Indeed, Monte Carlo (MC) and Phase Field Model (PFM) simulations [98,100-102] showed that the grain containing sub-boundaries of very low energy had an exclusively high probability of solid-state wetting and undergo selective AGG. The most important aspect of these simulations is that AGG is shown to occur by sub-boundaries even though the abnormally-growing grain was not given any advantage in terms of grain boundary mobility or energy. In other words, sub-boundaries induce AGG under a very realistic condition of grain boundary mobility or energy distribution.

## 1.5 The Possibility of having sub-boundary in Goss grains

There have been extensive studies as to the origin of Goss grains. The Goss grains are formed in the sub-surface region of the hot rolled sheet by shear deformation [42, 80-82]. When the sub-surface layer of the hot-rolled sample containing the Goss grains was removed, AGG occurred incompletely during secondary recrystallization [39, 83]. In addition, Duggan et al. [84] reported that if the near surface area in the primary recrystallized sheet was removed, the secondary recrystallization of the Goss texture did not occur during further annealing. Therefore, it is generally agreed that the Goss grains in the sub-surface region play an important role in secondary recrystallization.

During cold rolling, most of Goss grains are deformed and changed to other orientations. As a result, Goss grains are very rare after cold rolling and primary recrystallization, which makes it difficult to trace the microstructural evolution of the Goss grains. If Goss single crystals are used, however, this difficulty would be overcome to a degree. Mishra et al. [82] justified this approach by reporting that large Goss grains which are present in the sub-surface region after hot rolling qualitatively behave like Goss-oriented single crystals. Dunn [85] observed that when the Goss-oriented single crystal is used, the volume fraction of Goss grains after cold-rolling and primary recrystallization is much higher than that of the industrially processed polycrystalline Fe-3%Si steel. Therefore many studies on the origin of Goss grains were made using Goss-oriented single crystals [86-88].

There are two types of Goss grains in the sub-surface region. One is the Goss grains formed by shear during hot rolling. Some of these Goss grains survive during cold

rolling. The region where this type of Goss grains is situated after cold rolling is called ‘microbands’. The other is the Goss grains formed by shear during cold rolling. The region where this type of Goss grains is situated after cold rolling is called ‘shear bands’. Haratani et al. [88] and Ushioda and Hutchinson [87] suggested that Goss grains in shear bands formed during cold rolling is critical to the evolution of the strong Goss texture during secondary recrystallization.

Dorner et al. [71, 86, 89] observed the Goss component after cold rolling and identified microbands and shear bands. One type of Goss grains situated in shear bands was developed by high thickness reduction. The other type of Goss regions situated in microbands had been formed by hot rolling and survived after cold rolling. They observed that the Goss grains in microbands were evolved into AGG whereas the Goss grains in shear bands mostly disappeared during annealing. Based on this observation, they suggested that Goss grains between microbands became Goss nuclei of secondary recrystallization instead of Goss grain in shear bands.

According to sub-boundary enhanced solid-state wetting, the existence of sub-boundaries in Goss grains is critical for secondary recrystallization. Therefore, the origin of sub-boundaries in Goss grains needs to be examined in relation with the origin of Goss nuclei. Since Dorner et al.’s result [71] indicates that Goss nuclei are originated from the Goss grains formed by shear deformation during hot rolling, it should be examined how the sub-boundaries are formed exclusively in those Goss grains during cold rolling and primary recrystallization.

One scenario that can be thought of would be that Goss grains which survived after cold rolling have such low stored energy that they do not undergo recrystallization but undergo only recovery, producing dislocation boundaries or sub-boundaries. The

reason why grains of other orientations do not have sub-boundaries would be that after cold rolling they have such high stored energy as to induce recrystallization, producing mainly high angle boundaries.

Therefore, it needs to be confirmed whether Goss grains have low stored energy compared to grains of other major orientations after cold rolling. Motivated by this background, Park et al. [90] examined such a possibility using crystal plasticity finite element method (CP-FEM) under a plane strain condition. Since all orientations cannot be examined to identify the orientation of the lowest stored energy, calculations were limited to some representative orientations of Fe-3%Si steel. They reported that even though Goss and rotated cube orientations have the same Taylor factor which is the lowest value in the body-centered cubic (BCC) lattice, the Goss orientation has much lower stored energy. The reasons for this is that Goss orientation has a positive reorientation rate vector field divergence during plane strain deformation [11], which makes Goss accommodate easily the given deformation and as a result, the undeformed interior region of Goss has very low stored energy. Therefore, Goss orientation can have a minimally deformed region in comparison with other orientations. This is why Goss orientation can have a region of much lower stored energy than that of rotated cube which has the same Taylor factor. The CP-FEM calculations support the scenario that Goss grains that survived after cold work would have the lowest stored energy and undergo only recovery during primary recrystallization, producing sub-boundaries which enhance solid state wetting and result in selective AGG.

# Chapter 2. Synchrotron X-ray microdiffraction study focusing on sub-boundaries within abnormally growing grain in metallic materials

## 2.1 Observation of sub-boundaries inside Goss-oriented grains in Fe-3%Si steel

According to the concept of sub-boundary enhanced solid-state wetting, the selective Goss AGG occurs in Fe-3%Si steel because Goss grains should have the sub-boundaries exclusively. Therefore, it is necessary to confirm experimentally that abnormally-growing Goss grains in Fe-3%Si steel have sub-boundaries. Although the experiments had not been intended for this purpose, two groups reported that Goss grains in Fe-3%Si steel have a distinctive feature of having sub-boundaries of very low angle misorientation. The first group is Ushigami et al. [91, 92], who had made in-situ measurements by detailed synchrotron X-ray topography of Goss grains during AGG, discovered that Goss grains were divided into several sub-grains whose grain boundaries have a very low misorientation angle. The sub-boundaries were developed radially from a central site, which means that abnormally growing Goss grains have sub-boundaries at an initial stage of growth. Using synchrotron X-ray topography and transmission electron microscope (TEM), they measured misorientations of sub-boundaries of abnormally-growing Goss grains to be even less than 0.1° such as 0.04° and 0.09°. The second group is Dorner et al. [71], who

deformed a Goss-oriented single crystal up to 89% thickness reduction and subsequently annealed it. The texture of a Goss-oriented single crystal after 89 % of cold rolling is characterized by two major γ-fiber {111}<112> components and a minor {110}<001> Goss component. However, during annealing a strong Goss texture develops. Within the recrystallized Goss grains, they discovered very small-angle grain boundaries with some misorientations even significantly smaller than 1°.

Since such previous discoveries that Goss grains exclusively have sub-boundaries were made not purposefully but rather accidentally, the observation more objectively supports the mechanism of sub-boundary enhanced solid-state wetting. Motivated by these backgrounds, Park et al. [93] made extensive TEM observations of abnormally growing Goss grains as well as matrix grains in Fe-3%Si steel in the initial stage of secondary recrystallization with a purpose of checking whether sub-boundaries are a unique feature of Goss grains or not. To obtain statistically meaningful data, they examined 10 abnormally-growing Goss grains and 100 matrix grains. Without exception, they observed sub-boundaries which have an aligned edge dislocation structure in abnormally growing Goss grains but could not observe such sub-boundaries in matrix grains. From the dislocation spacing of sub-boundaries observed by annular dark field scanning TEM (ADF-STEM), they determined the misorientation angle of sub-boundaries to be 0.15° and 0.17°. If sub-boundary enhanced solid-state wetting is responsible for AGG in Fe-3%Si steel, the same mechanism would apply to other systems. This means that abnormally growing grains in other systems would also have sub-boundaries. In order to confirm this, Park et al. [94] made TEM observations of 7 abnormally growing grains and 100 matrix grains in Al 5052 alloy. Among 7 abnormally growing grains and 100 matrix

grains examined by TEM, without exception all abnormally growing grains had sub-boundaries but matrix grains had not. The misorientation angles of the sub-boundaries inside abnormally growing grains in Al 5052 alloy was estimated as 0.22° and 0.29°.

All these results imply the possibility that Goss grains should have a unique feature of having sub-boundaries, which is responsible for selective AGG. Therefore, it is worth studying this possibility in more detail. The observation by TEM is limited to such a small area that it might not be representative of the entire sample and it is difficult to draw a general conclusion. The purpose of this study is to investigate the sub-boundaries in the entire area including Goss grains and matrix grains of sample, which underwent the initial stage of secondary recrystallization, using a proper method having high resolution and ability to investigate a large area.

## 2.2 EBSD analysis with Kernal Average Misorientation focused on the observation of sub-boundary

One of possible methods for the observation of sub-boundary with analyzing relatively large area as well as high angular resolution is EBSD. The EBSD technique has been automated and intensively developed during the two last decades in terms of indexing speed and accuracy [95]. It has been generally known that Kernel average misorientation (KAM) during EBSD analysis can be used for the measurement of local grain misorientation. KAM is the average misorientation angle around a given scan point with respect to a defined set of nearest neighbor points. Recently many studies [96, 97] related with deformation substructure were made using KAM method because this value helps to understand local lattice distortions, localized deformation and dislocation density. Sub-boundary which is formed by polygonization of dislocation can influence on lattice misorientation locally in grain, so we analyzed Goss grains and neighboring matrix grains in the initial stage of secondary recrystallization in Fe-3%si steel using this tool.

EBSD analysis was done in collaboration with Dr. Joo-Hee Kang at Korea institute of materials science (KIMS). The specimen was electrolytic polished and analyzed by EBSD. EBSD detector used in this study was NordlysNano (Oxford) which has high angular resolution less than 0.1°.

Fig. 2.1 shows the microstructure of Goss grain and neighboring matrix grains at initial stage of abnormal grain growth in Fe-3%Si steel. It is shown in Fig. 2.1(c) that small KAM value below 1° are observed in Goss grains. However, it seems that these local misorientation inside Goss grains are caused by topology of surface, not by

sub-boundary when the KAM map shown in Fig. 2.1(c) is compared with forward scatter diffraction (FSD) images which shows the topology and orientation (Fig. 2.1(b)). It is known that EBSD analysis is sensitive to surface of specimen because electron probe has low penetration depth. Thus, other method was needed in order to investigate sub-boundary without uncertainty.

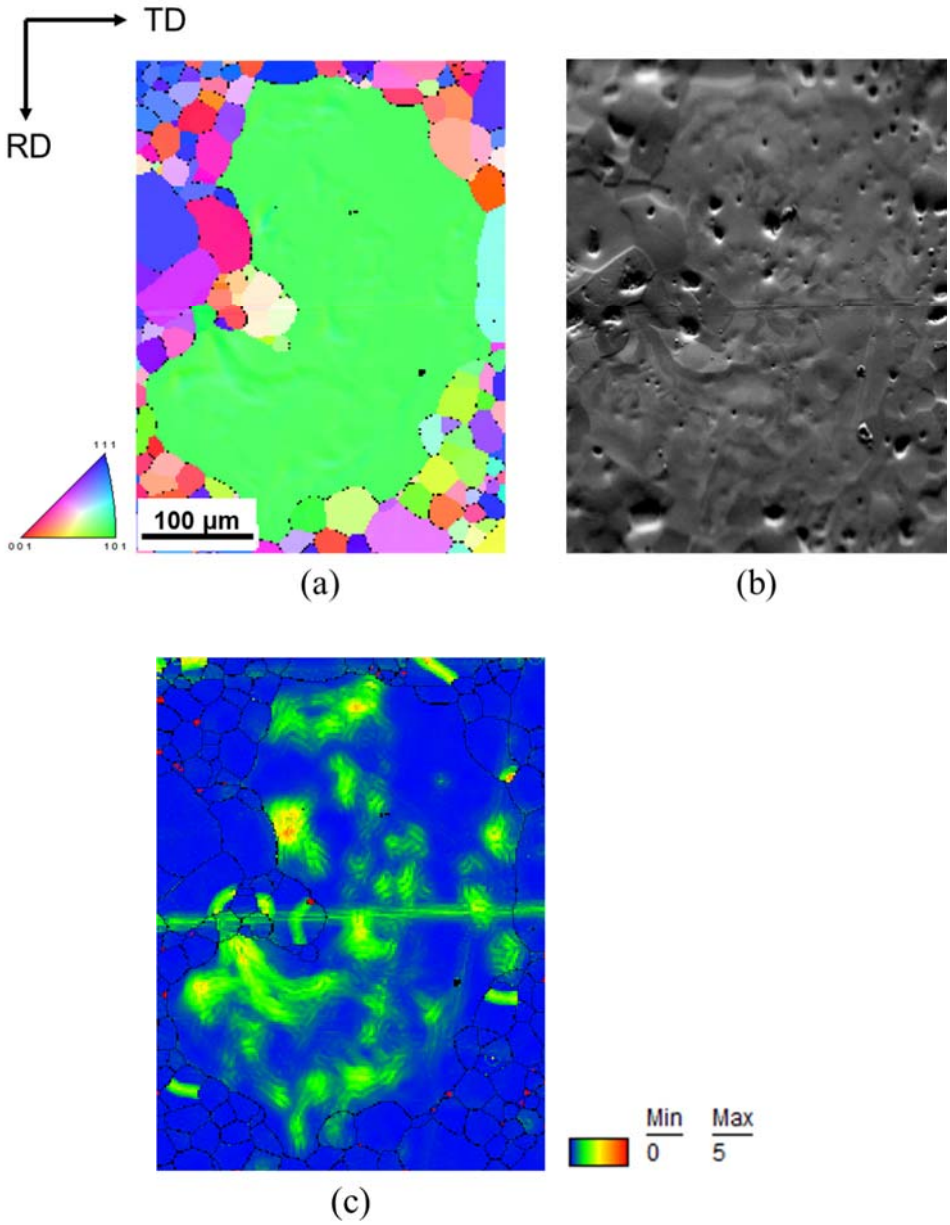


**Fig. 2.1.** The microstructure of Goss grain and neighboring grains at initial stage of abnormal grain growth in Fe-3%Si steel. (a) Inverse pole figure map (b) FSD image (c) KAM map

## 2.3 Synchrotron X-ray microdiffraction

In general, X-ray diffraction analysis has been known as powerful technique to study the structural properties of materials because X-ray has a wavelength which has the order of the interplanar spacing of crystalline materials. X-ray diffraction techniques yield the valuable information such as crystal structure, crystallographic orientation, interplanar spacing of specific crystal plane and so on [98]. Also, X-ray probe has advantage of deeper penetration depth in comparison with the electron probes, so that bulk specimens can be investigated. However, X-ray diffraction analysis has been limited by spatial resolution of the X-ray probe.

The developments of high-brilliant third generation synchrotron source and the advances in X-ray optics and in detecting techniques created x-ray probe of submicron size and made it possible to study material properties with outstanding spatial and angular resolution [99-101]. In other words, it is possible to scan specimens obtain maps of grain orientation, stress/strain distribution with high spatial and angular resolution. Mapping of grain orientation can be also obtained by EBSD, but the synchrotron x-ray microdiffraction is superior to EBSD analysis in strain/stress sensitivity, accuracy for grain-orientation measurement and depth-probing ability [102]. In addition, synchrotron X-ray microdiffraction is a non-destructive analysis and has an advantage of scanning a large area in comparison with TEM.

Thus, the synchrotron X-ray microdiffraction is determined to suitable method for our objective to study sub-boundaries through the entire sample with high angular resolution.

## 2.4 Experimental procedure

An ingot of Fe-3wt%Si steel was used as a starting material which contains aluminum nitride (AlN) as a grain growth inhibitor to manufacture the highly grain oriented electrical steel. The ingot was hot rolled to 2.3 mm and cold rolled to 0.3 mm thickness. After primary recrystallization, the steel sheets were heated up to 1060 ℃ at 5 ℃/min, held 0 s and cooled to room temperature to produce a microstructure at the initial stage of secondary recrystallization. Then the sheets were chemically etched with 65% $H_2O$-35%HCl at 100 ℃. The microstructure was observed by optical microscopy (Eclipse L150, Nikon) to identify Goss grains which underwent the initial stage of AGG and the abnormally grown Goss grains as large as ~ 300 μm were selected for the analysis. For the statistical reliability, 5 Goss grains and 1400 matrix grains near the Goss grains are examined.

Synchrotron white beam x-ray microdiffraction experiments were conducted on 4B beamline, which has a geometry of Laue diffraction, at the Pohang Accelerator Laboratory (PAL). Fig. 2.2 shows a schematic of the microdiffraction beamline and the real experimental configuration of beamline in 4b beamline at PAL. The incident white beam was focused to 1 μm × 1 μm using a Kirkpatrick-Baez (K-B) mirror system, and the sample was mounted on a stage in a 45° reflective geometry. Laue diffraction images were recorded by a charged coupled device (CCD) X-ray detector (Bruker APEX II). Additional details on experimental setup are mentioned elsewhere [101]. The area including a Goss grain and matrix grains was scanned two dimensionally with a step size of 4 μm. Laue diffraction images were collected at

each step, so that about 10000 images per one sample were used for analysis. The geometrical calibration for calculating the exact orientation of grains was done using an unstrained Ge (111) single crystal. Based on Laue diffraction data, Software called XMAS (X-ray microdiffraction analysis software) [99, 101] was used for indexing Laue diffraction peaks, calculating orientation, analyzing Laue diffraction peaks, and resolving the distortion problem caused by using the flat CCD detector to detect the Laue diffraction peaks in a three dimensional space [98]. Details including algorithms of peak indexing and calculating orientation in the software are described elsewhere [103].

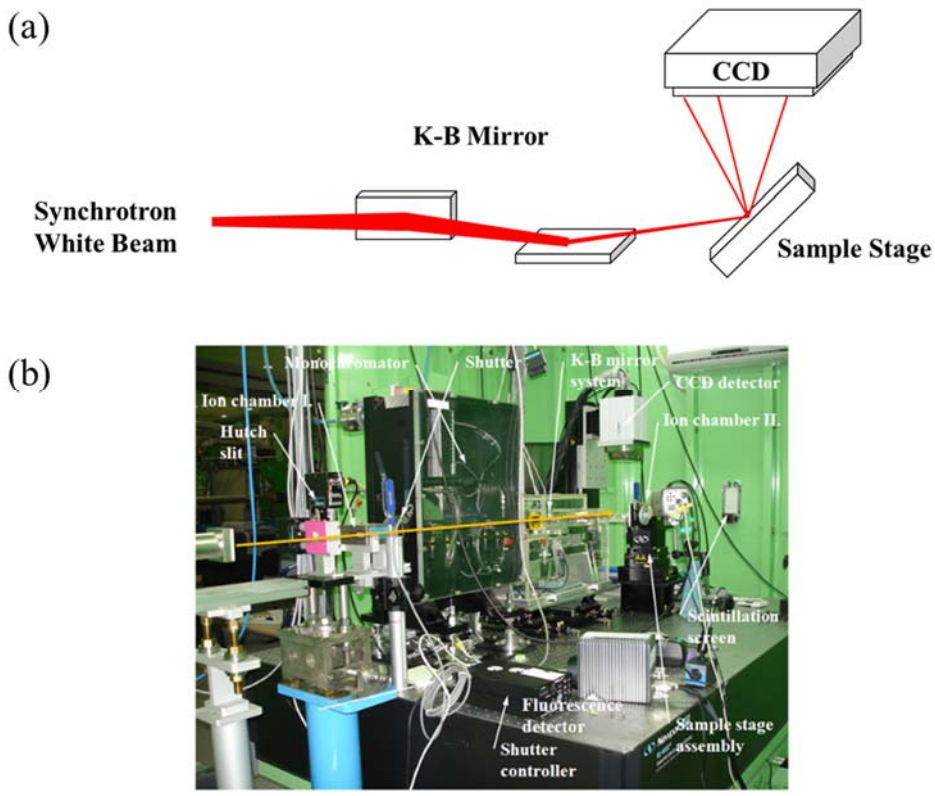


**Fig. 2.2.** The experimental configuration of synchrotron X-ray microdiffraction in 4B beamline at PAL. (a) The schematic (b) the real configuration

## 2.5 The observation of sub-boundary approached by splitting of Laue diffraction peaks

Because a sub-boundary consists of dislocations aligned through polygonization, it has an effect on the shape of diffraction patterns. Fig. 2.3 illustrates how the sub-boundary affects a Laue diffraction peak. The Laue diffraction peak has a spherical shape (Fig. 2.3(b) 'I') when the incident beam is diffracted at an area without a sub-boundary (Fig. 2.3(a) 'I'). If the incident beam is diffracted at an area containing the sub-boundary (Fig. 2.3(a) 'II'), however, the Laue peak shows a splitted shape that consists of two maxima having a very low deviation (Fig. 2.3(b) 'II'). According to Barabash et al. [104-106], who intensively studied the synchrotron white beam microdiffraction for the quantitative analysis of dislocation structures, geometrically necessary boundaries (GNB) formed by the alignment of unpaired geometrically necessary dislocations (GND) through polygonization, which is equivalent to sub-boundaries, cause Laue diffraction peaks to split through both simulations and experiments. Therefore, splitting of Laue peaks in synchrotron X-ray microdiffraction experiments is regarded as the indication of sub-boundaries as reported by Budiman et al. [107] in their study of Cu damascene interconnect lines during electromigration.

Based on this correlation between the splitting of Laue peaks and the sub-boundary, we are going to analyze all grains in the scanned area focusing on the existence of sub-boundaries. Laue diffraction peaks are expressed in the $\chi$-$\theta$ space where $\chi$ is the angle of the diffracted beam within the plane perpendicular to the incident beam and $\theta$ is the Bragg angle [99].

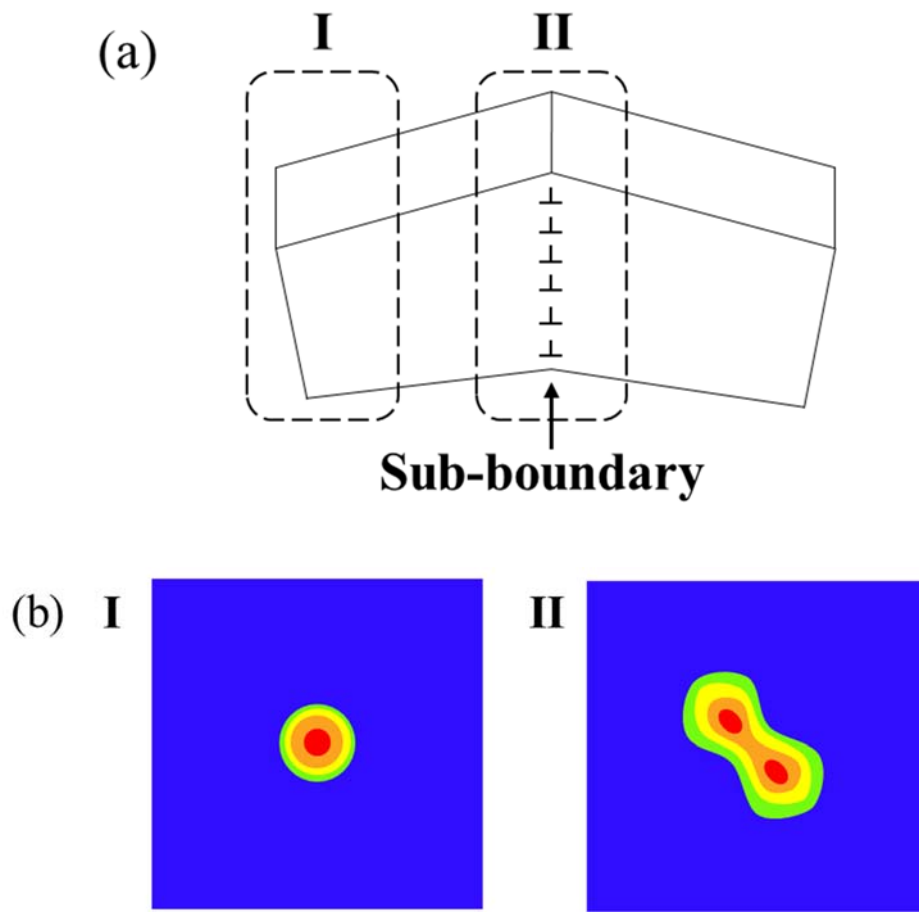


**Fig. 2.3.** (a) Schematic of crystal which has a sub-boundary. (b) Shape of Laue diffraction peaks between the area without (I) and with (II) sub-boundary.

## 2.6 Sub-boundaries inside Goss grains in Fe-3%Si steel

Fig. 2.4(a) shows microstructures of two Goss grains at the initial stage of AGG. In order to represent graphically the orientations of grains in microstructures calculated from XMAS, an electron backscatter diffraction (EBSD) software (TSL OIM) was used to produce an inverse pole figure map of Fig. 2.4(a). Among all the area investigated, four locations in Fig. 2.4(a) are indicated as A, B, C and D, which correspond respectively to the splitted (011) Laue diffraction peaks of A, B, C and D in Fig. 2.4(b), which again correspond respectively to the intensity profiles of A, B, C and D in Fig. 2.5. All the four Laue diffraction peaks are splitted into two maxima in Fig. 2.4(b) and Fig. 2.5. This means that there are sub-boundaries in two Goss grains in Fig. 2.4(a).

Among 5 large Goss grains and 1400 matrix grains examined in this study, only 5 Goss grains, which underwent the initial stage of AGG, showed splitted Laue diffraction peaks whereas none of matrix grains showed a splitted peak without exception. Considering that the peak splitting indicates the existence of a sub-boundary, it can be said that a sub-boundary is a distinctive feature of Goss grains undergoing AGG in Fe-3wt%Si steel. Ushigami et al. [91, 92] also reported the exclusive existence of sub-boundaries in Goss grains during AGG by observing substructures in Goss grains, which were divided into subgrains with sub-boundaries having a very low misorientation angle less than 0.5° using in-situ synchrotron X-ray topography. Dorner et al. [71] also reported that only Goss grains have sub-boundaries with misorientation angles below 1° after primary recrystallization of the cold rolled sample of a single crystal with Goss orientation. In addition, Park et al.

[93] directly observed sub-boundaries which consist of an array of edge dislocations and have misorientation angles below 0.5° through extensive TEM analyses.

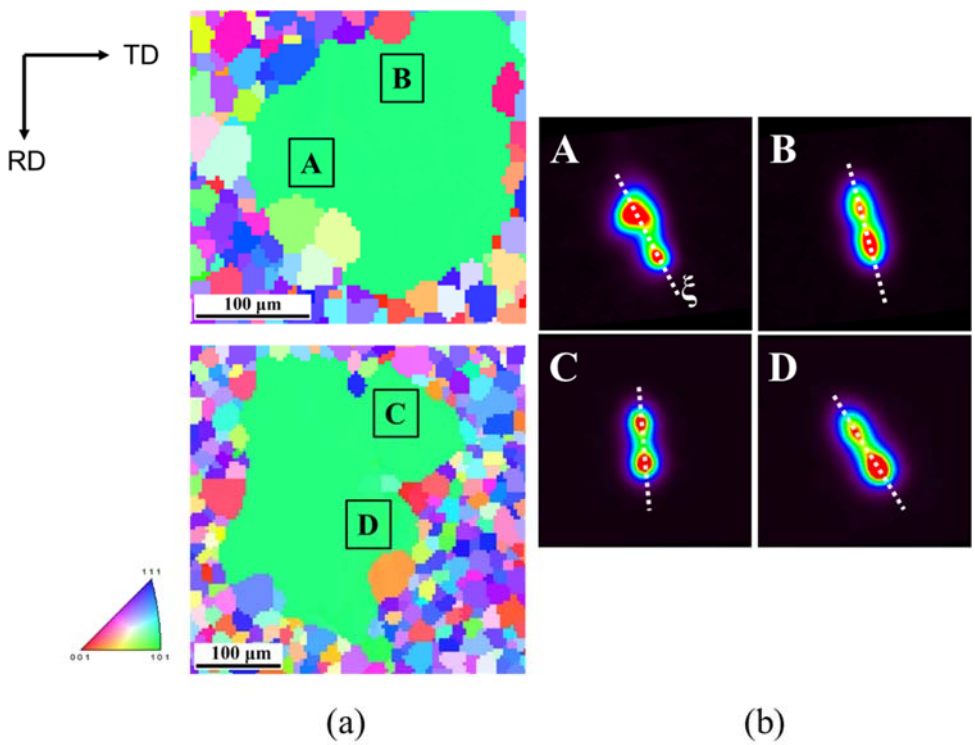


**Fig. 2.4.** (a) Microstructures of Goss grains at the initial stage of AGG. (b) Splitting of (011) Laue diffraction peaks in θ-χ space at four locations (A, B, C and D) in abnormally growing Goss grains.

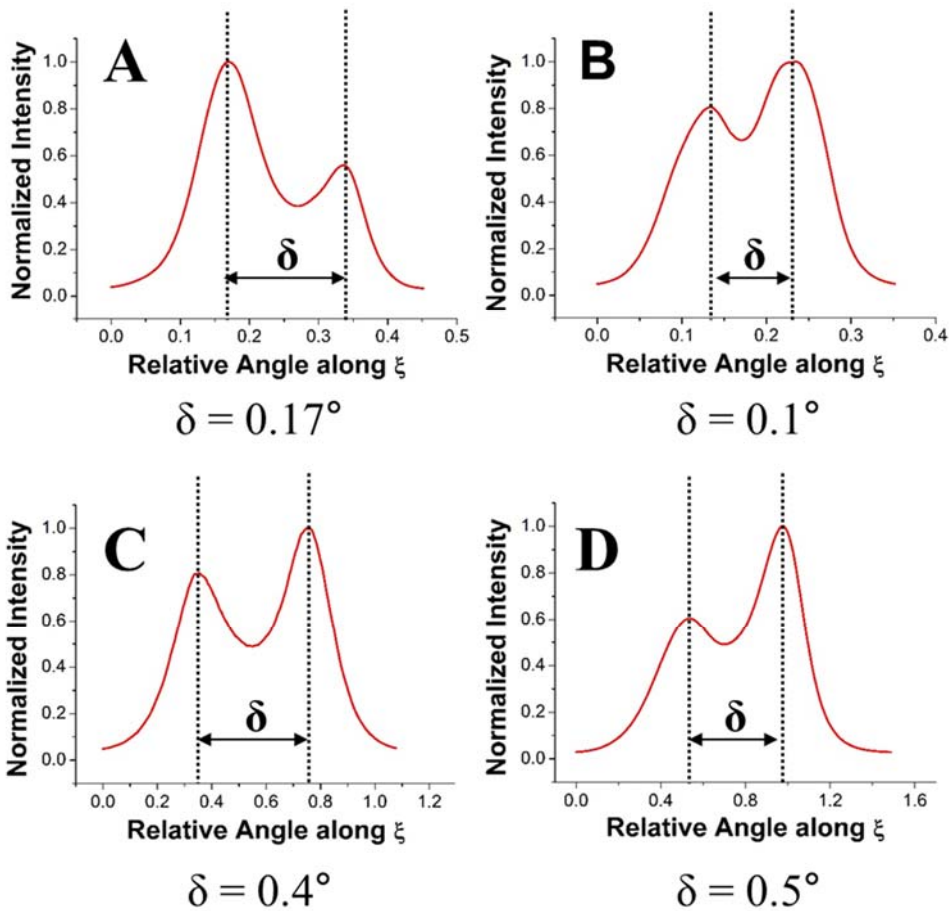


**Fig. 2.5.** Intensity profiles along the direction ξ at four locations (A, B, C and D) in abnormally growing Goss grains.

The misorientation angle of sub-boundary can be calculated from the deviation between the intensity maxima along the spilt direction ξ [104-106]. Intensity profiles along the ξ direction were plotted in Fig. 2.5 to determine misorientation angles of sub-boundaries. Misorientation angles of subgrain boundaries in positions A, B, C and D were calculated to be respectively 0.17°, 0.1°, 0.4° and 0.5°. Other Goss grains in this study also had sub-boundaries that have misorientation angles less than 0.6°.

In addition to calculating misorientation angles, the synchrotron X-ray microdiffraction can be used to investigate additional information as to dislocations forming sub-boundaries. Unpaired GNDs and GNBs in crystal cause streaking and splitting of Laue diffraction peaks respectively [99, 100]. Also, the Burgers vector b and the direction of dislocation line τ of GNDs can be found from the direction of streaking [107]. Since sub-boundaries, which are equivalent to GNBs, are formed by the alignment of unpaired GNDs, it is possible to estimate the feature of sub-boundaries from the direction of peak splitting in Laue diffraction patterns. Based on results of Park et al. [93] that sub-boundaries in Goss grains consisted of edge dislocations, Laue diffraction patterns of Goss grains simulated by XMAS for 48 slip systems in BCC crystals were compared with our experimental data. Table 2.1 shows the characteristics of sub-boundaries observed at four locations in Goss grains in Figure 2.4(a). Dislocations aligned in sub-boundaries were found to have Burgers vector b for 1/2<111> family which is a principal slip direction of body-centered cubic (BCC) [108]. Since misorientation angle δ and Burgers vector b are determined, dislocation spacing h within the sub-boundary could also be calculated using equation $\delta \fallingdotseq b/h$ [109] as listed in Table 2.1. From these results, the misorientation angle of the sub-boundary could be determined as 0.17° around $[2\bar{1}\bar{1}]$ axis, which

is equivalent to the directions of dislocation line τ, and dislocations in the sub-boundary has spacing with 83.67 nm in case of the location A in Figure 2.4(a). Other Goss grains in this study had 1/2<111> family for b and <211>, <514>, <110> families for τ.

| Positions | δ (°) | **b** | **τ** | d (nm) |
|---|---|---|---|---|
| A | 0.17 | ½[$\bar{1}$ 1 $\bar{1}$] | [$\bar{2}$ $\bar{1}$ 1] | 83.67 |
| B | 0.1 | ½[$\bar{1}$ 1 $\bar{1}$] | [5 1 $\bar{4}$] | 142.23 |
| C | 0.4 | ½[$\bar{1}$ 1 1] | [$\bar{4}$ 1 $\bar{5}$] | 35.55 |
| D | 0.5 | ½[$\bar{1}$ 1 1] | [$\bar{2}$ $\bar{1}$ $\bar{1}$] | 28.45 |

**Table 2.1.** Characteristics of sub-boundaries at four locations (A, B, C and D) in Fig. 2.4(a).

In order to estimate the distribution and the morphology of sub-boundaries, all positions where splitting of Laue diffraction peaks occurred were marked as shown illustrated in Figure 2.6. The morphology of sub-boundaries was broad rather than sharp, which is attributed to the fact that the penetration depth of X-ray is approximately 40 μm and the sub-boundary plane is not perpendicular to the normal direction of the sample. It is observed that sub-boundaries which have misorientation angles below 0.6° distributed inhomogeneously in Goss grains.

It is possible that sub-boundaries, which are observed in Goss grains, may not result from the recovery in primary recrystallization but be formed due to the orientation gradient within Goss grains resulting from grain growth of Goss grains into a large size. If there exists an orientation gradient, there would be a lattice gradient within the grain, which would have an influence on the diffraction peaks. Then, the

positions of diffraction peaks corresponding to Goss grains would move gradually when the position of the Laue diffraction peaks was traced along the specific scanning direction. Also, the streaking phenomena of Laue diffraction peaks with a continuous intensity profile would be observed if there is an orientation gradient in large Goss grains. Considering these possibilities, we analyzed all the grains in the scanned area, focusing on the movement and streaking as well as splitting of Laue diffraction peaks. However, neither gradual movements of Laue diffraction peaks nor streaking of diffraction peaks with a continuous intensity profile was observed in Goss grains, which means that the orientation gradient accompanied by the growth of Goss grains was not detected in this study.

In this work, the sub-boundaries were observed to exist in the abnormally-growing Goss grains. It would have been more convincing if the observations were made on the primary recrystallized sample before the onset of AGG. However, this experiment turns out to be very difficult because the fraction of Goss grains in the primary recrystallized sample is only ~ 1% and besides, only a few of these Goss grains undergo AGG. In order to identify Goss grains, the sample should be polished for the orientation determination by EBSD. Then, the polishing procedure might slightly deform the surface and affect the microdiffraction result.

On the other hand, Dorner et al. [71], who investigated the origin of abnormally growing Goss grains in detail, reported that Goss grains have a unique feature of having subgrain boundaries with misorientation angles below 1° after primary recrystallization of the cold rolled sample of the single crystal Fe-3%Si steel with Goss orientation. They could determine such small misorientation angles using kernel average misorientation (KAM). According to them [86], Goss grains exist

both in microbands and shear bands. They observed that only Goss grains in microbands had sub-boundaries and grew abnormally whereas Goss grains in shear bands had been previously believed to be the origin of abnormally growing grains.

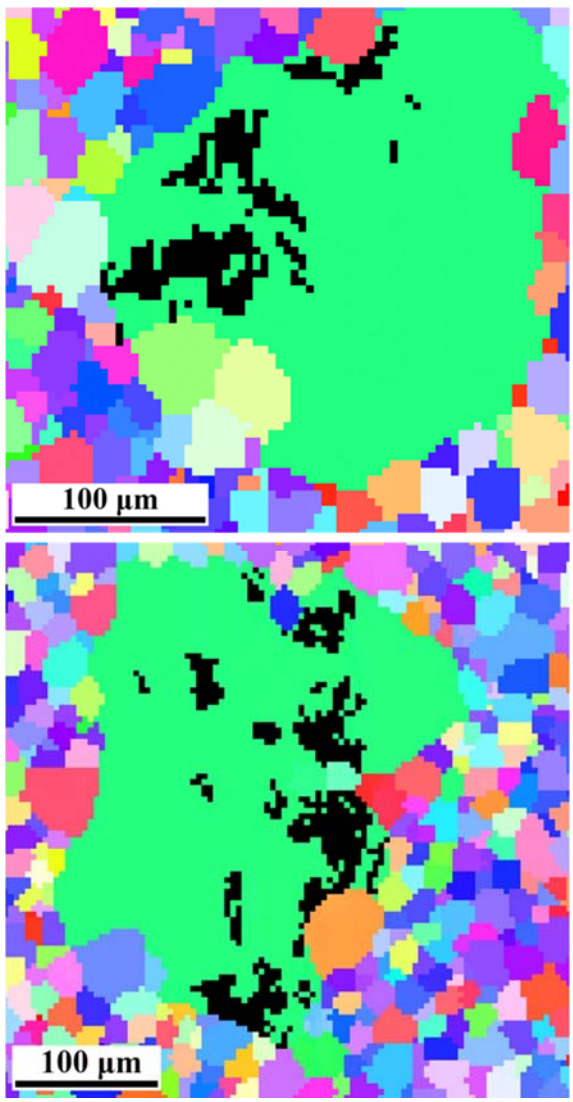


**Fig. 2.6.** Distribution of sub-boundaries in abnormally growing Goss grains expressed by marking positions where splitting of Laue peaks occurs.

# Chapter 3. Abnormal grain growth induced by low deformation in Fe-3%Si steel

## 3.1 Introduction

As mentioned in Chapter 2, sub-boundaries is the exclusive feature of abnormally growing Goss grains in Fe-3%Si steel as shown in this study as well as other literatures. In other words, these results implies that the sub-boundaries should play an important role in selective AGG of Goss grains in Fe-3wt%Si steel. If the suggestions that AGG occurs by solid-state wetting mechanism and that sub-boundary plays a key role in selective AGG are reasonable, the grains which do not have Goss orientation should undergo AGG during annealing, as shown in Fig. 3.1, when we form sub-boundaries in those grains artificially in Fe-3%Si steel where the only Goss oriented grains undergo AGG.

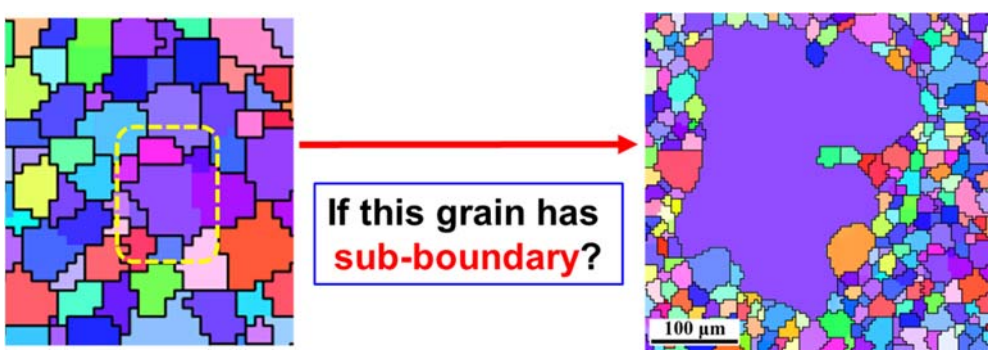


**Fig. 3.1.** The possibility for the abnormal grain growth of non-Goss grain by formation of sub-boundary.

One of method which can form sub-boundaries inside grains is inducing recovery process. It is generally known that metals undergo recovery through polygonization of dislocations when the metals is annealed after low deformation because they have not sufficient stored energy which is the driving force for recrystallization [110].

In this point of view, AGG behavior of non-Goss grains was investigated in Fe-3%Si steel when sub-boundaries were formed in non-Goss grains by method of local deformation through indentation after primary recrystallization.

## 3.2 Experimental Procedure

An ingot of Fe-3wt%Si steel was used as a starting material which contains aluminum nitride (AlN) as a grain growth inhibitor to manufacture the highly grain oriented electrical steel. The ingot was hot rolled to 2.3 mm and cold rolled to 0.3 mm thickness. After primary recrystallization, indentation was performed to the specimen under the loads of 3, 6, 12 and 18 kgf and the specimens undergo primary recrystallization again at 860 °C for 10 min in order to form sub-boundary by recovery process. Then the specimens were heated up to 1080 °C at 5 °C /min, held 0 s and cooled to room temperature to produce a microstructure at the initial stage of secondary recrystallization. Then the sheets were chemically etched with 65% $H_2O$-35% HCl at 100 °C. The microstructures of the specimens were observed by optical microscopy (Eclipse L150, Nikon) to identify abnormally grown grains near indentation mark.

In order to determine the orientation of abnormally grown grains and investigate that abnormally grown grains have sub-boundaries, synchrotron white beam x-ray microdiffraction experiments were conducted on 4B beamline, which has a geometry of Laue diffraction, at the Pohang Accelerator Laboratory (PAL). The incident white beam was focused to 1 μm × 1 μm using a Kirkpatrick-Baez (K-B) mirror system, and the sample was mounted on a stage in a 45° reflective geometry. Laue diffraction images were recorded by a charged coupled device (CCD) X-ray detector (Bruker APEX II). Additional details on experimental setup are mentioned elsewhere [101]. The area including an abnormally grown grain near the indentation mark and matrix grains was scanned two dimensionally with a step size of 7-9 μm. Laue diffraction

images were collected at each step, so that about 10000 images per one sample were used for analysis. The geometrical calibration for calculating the exact orientation of grains was done using an unstrained Ge (111) single crystal. Based on Laue diffraction data, Software called XMAS (X-ray microdiffraction analysis software) [99, 101] was used for indexing Laue diffraction peaks, calculating orientation, analyzing Laue diffraction peaks, and resolving the distortion problem caused by using the flat CCD detector to detect the Laue diffraction peaks in a three dimensional space [98]. Details including algorithms of peak indexing and calculating orientation in the software are described elsewhere [103].

## 3.3 Abnormal grain growth of non-Goss grains induced by low deformation

Fig 3.2 shows the microstructure of etched specimens after annealing. AGG occurred near the indentation mark in all specimens. When the specimens were deformed under low loads of 3 and 6 kgf, it seems that the only one grain underwent AGG during annealing. When the specimens were deformed under high loads of 12 and 18 kgf, on the other hand, it seems that two or more grains underwent AGG during annealing. In order to determine the crystallographic orientation of abnormally these grown grains and identify that abnormally grown grains have sub-boundary, the specimens were analyzed by synchrotron x-ray microdiffraction.

Fig. 3.3 shows the orientation maps of the specimens, which were analyzed using synchrotron x-ray microdiffraction. It is observed that all the abnormally grown grains did not have Goss orientation. At low load such as 3 and 6 kgf, One grain underwent AGG during annealing. On the other hand, three and eight grains grew abnormally at load of 12 and 18 kgf, respectively. It can be considered that abnormally grain growth of non-Goss orientation is caused by low deformation because only Goss grains undergo AGG during secondary recrystallization in Fe-3%Si steel in general. However, these results do not tell us that those non-Goss grains undergo AGG because they had sub-boundary. It is difficult to identify that abnormally grown grains which induced by low deformation have sub-boundaries through orientation map. Thus, Laue diffraction peaks of all grain s were investigated focusing on the splitting phenomena which indicate the existence of sub-boundary [111].

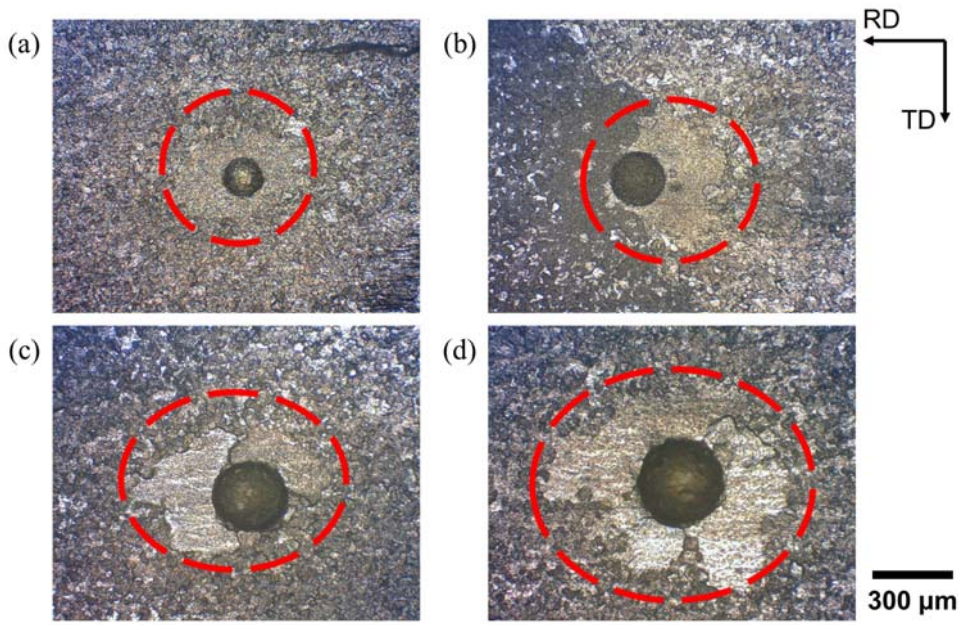


**Fig. 3.2.** The microstructures of chemically etched specimens after annealing. (a) 3 kgf, (b) 6 kgf, (c) 12 kgf and (d) 18 kgf.

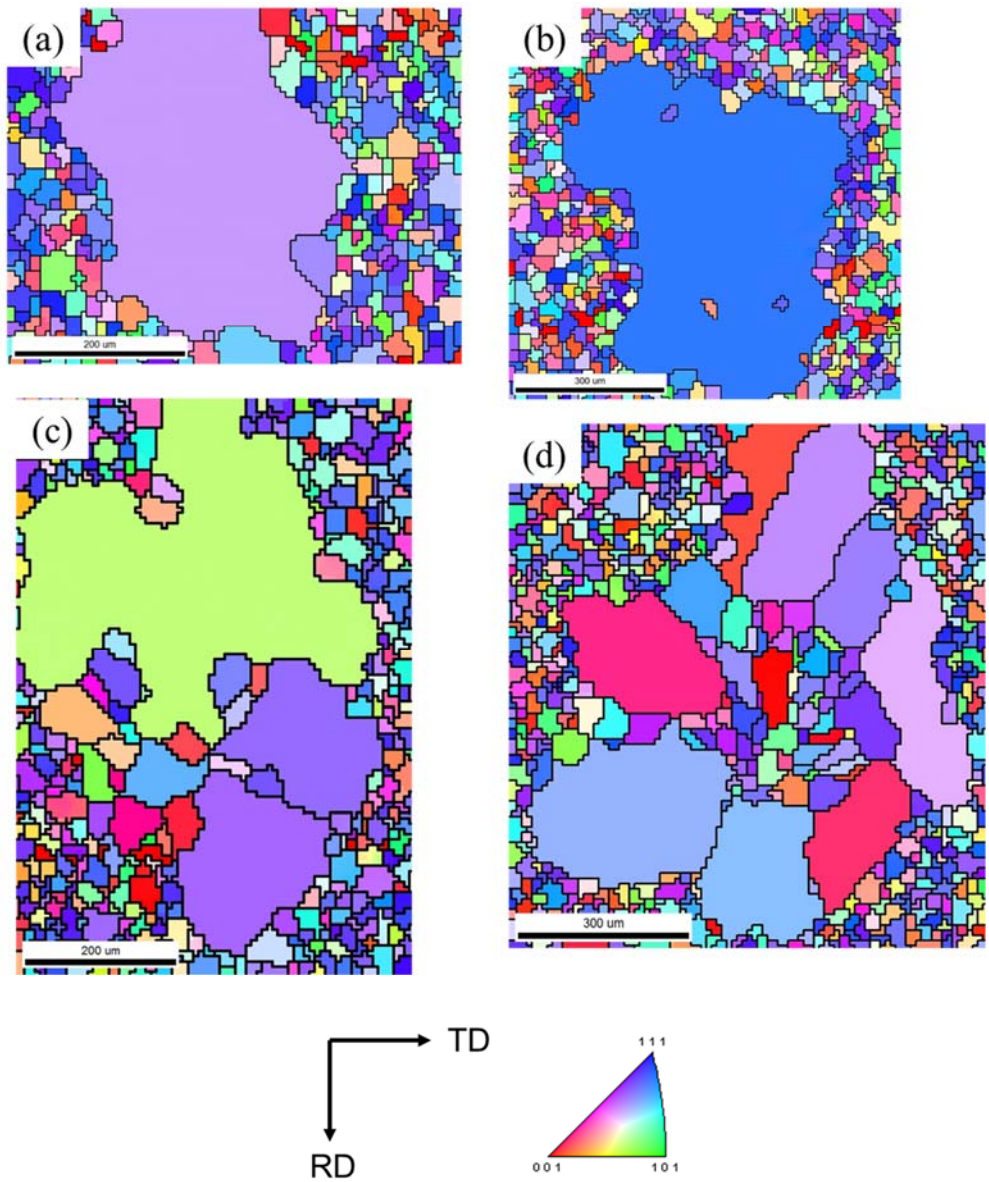


**Fig. 3.3.** Orientation maps analyzed by Synchrotron X-ray microdiffraction.

(a) 3 kgf, (b) 6 kgf, (c) 12 kgf and (d) 18 kgf

## 3.4 Sub-boundaries inside abnormally grown grains of non-Goss orientation induced by low deformation

Fig. 3.4 show the splitted $(\bar{1}\bar{1}4)$ Laue diffraction peaks inside abnormally grown grains of non-Goss orientation induced by low deformation under load of 3 kgf at specific locations, which indicate that the sub-boundaries exist inside abnormally grown grains. The misorientation angles of sub-boundaries observed inside abnormal grains were below 0.6°, which is similar with abnormally growing Goss grains in Chapter 2. The splitting of Laue diffraction peaks was also observed in all specimens that was deformed locally by indentation under 6 (Fig. 3.5), 12 (Fig. 3.6 and 3.7) and 18 kgf (Fig. 3.8 and 3.9). The sub-boundaries also have very low misorientation angle below 0.6°. It was found that all grains which underwent AGG have sub-boundary of very low misorientation angle and other matrix grains do not have sub-boundary without exception.

According to sub-boundary enhanced solid state wetting, sub-boundary plays a key role for selective AGG because sub-boundary increase the probability of solid-state wetting. Considering the fact that the sub-boundaries were observed inside all of abnormally grown grain which have non-Goss orientations, it can be considered that those grains underwent AGG because they have sub-boundaries which were induced by low deformation when they subjected to secondary recrystallization. Also, these results indicate that AGG occur by sub-boundary enhanced solid-state wetting. It is suggested that AGG of grains which are desired to grow could be controlled and texture could made by forming sub-boundaries based on sub-boundary enhanced solid-state wetting mechanism.

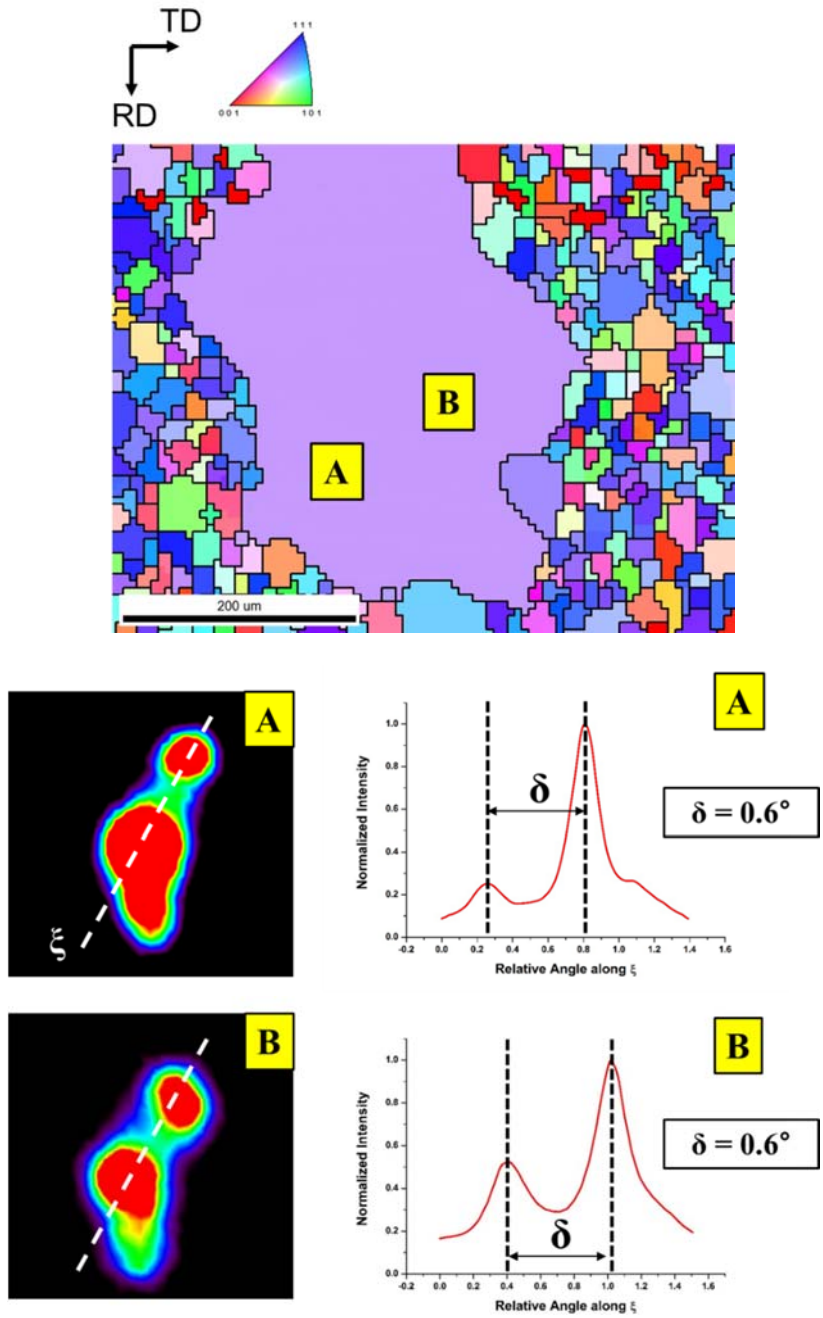


**Fig. 3.4.** Splitting of $(\bar{1}\,\bar{1}\,4)$ Laue diffraction peaks in θ-χ space and intensity profiles along the direction ξ at specific locations in abnormally growing grains induced by indentation under the load of 3 kgf.

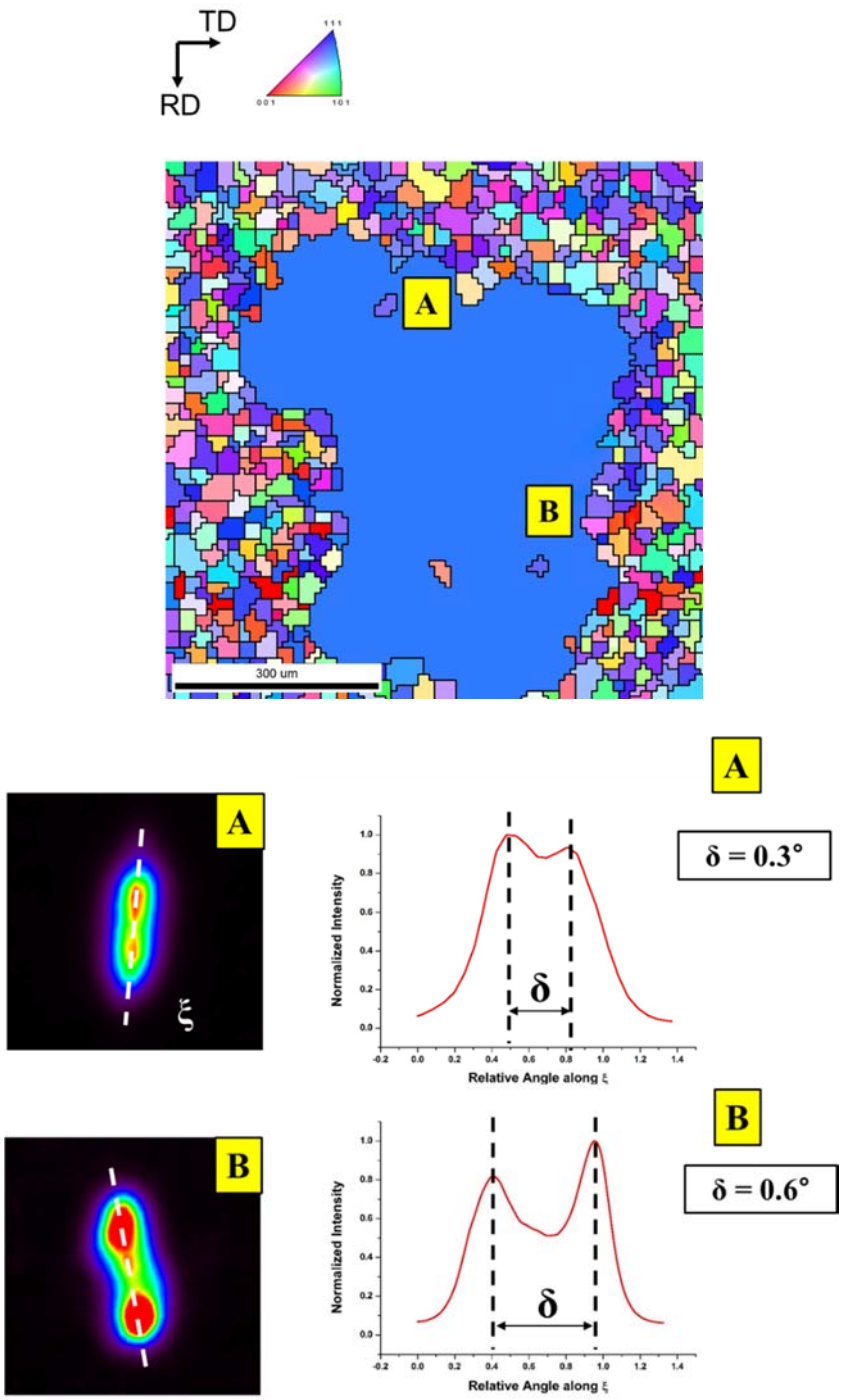


**Fig. 3.5.** Splitting of $(\bar{1}\,\bar{2}\,3)$ Laue diffraction peaks in θ-χ space and intensity profiles along the direction ξ at specific locations in abnormally growing grains induced by indentation under the load of 6 kgf.

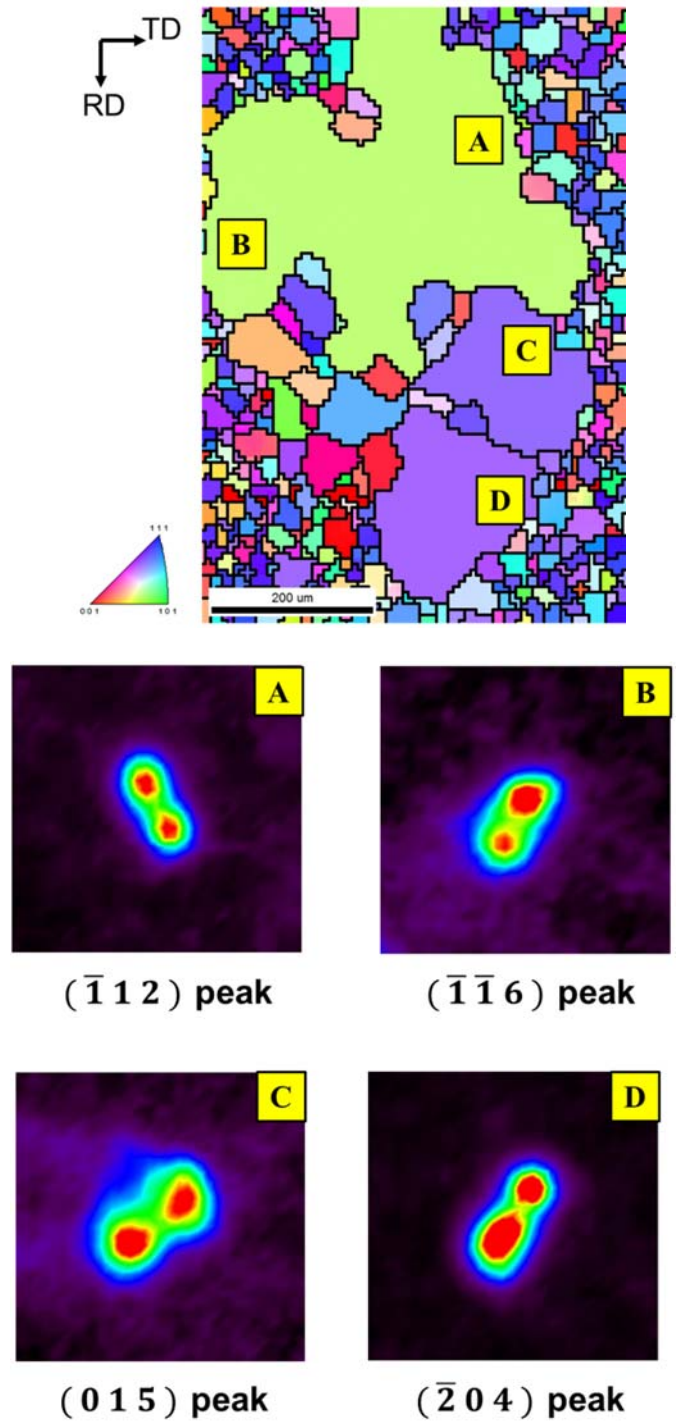


**Fig. 3.6.** Splitting of Laue diffraction peaks in θ-χ space at specific locations in abnormally growing grains induced by indentation under the load of 12 kgf.

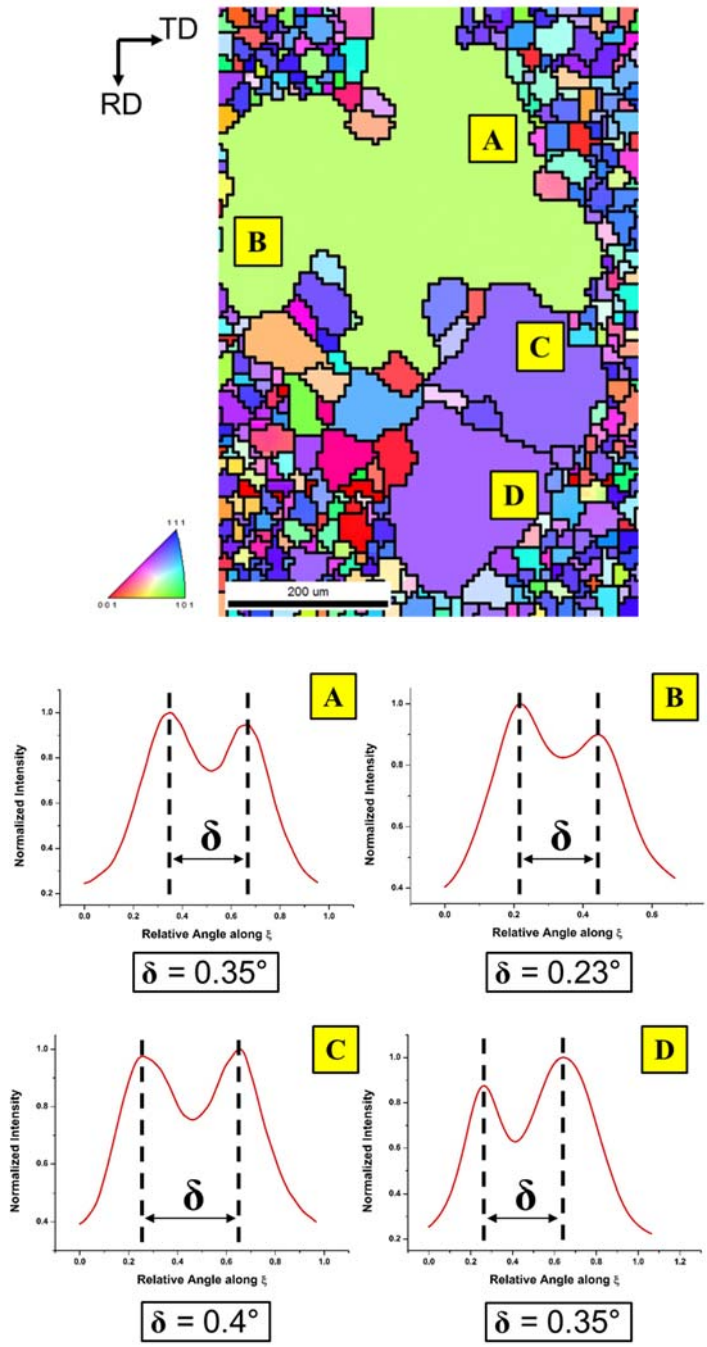


**Fig. 3.7.** Intensity profiles along the splitting direction of Laue diffraction peaks in Fig 3.6 at specific locations in abnormally growing grains induced by indentation under the load of 12 kgf.

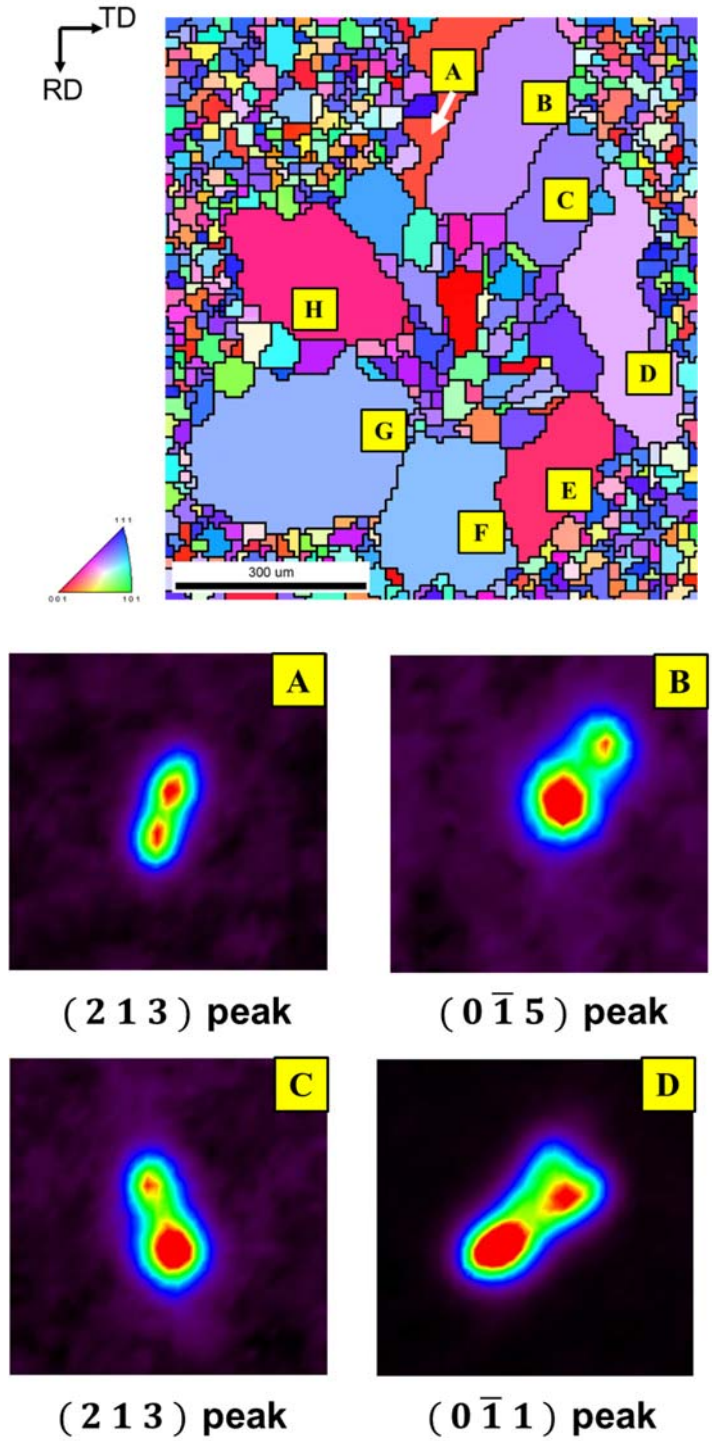


**Fig. 3.8.** Splitting of Laue diffraction peaks in θ-χ space at specific locations in abnormally growing grains induced by indentation under the load of 18 kgf.

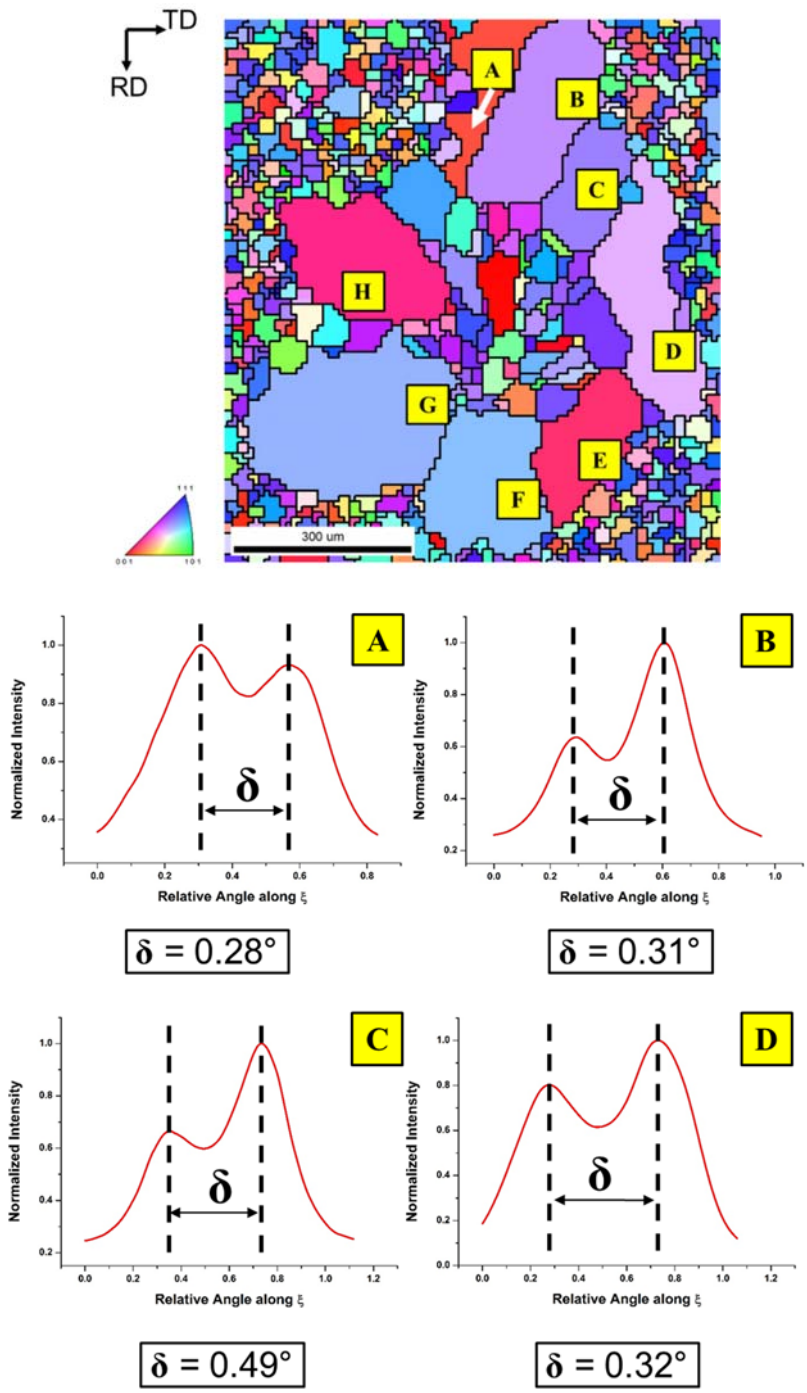


**Fig. 3.9.** Intensity profiles along the splitting direction of Laue diffraction peaks in Fig 3.8 at specific locations in abnormally growing grains induced by indentation under the load of 18 kgf.

# Part 2. Effects of external electric field on the microstructures in metallic materials

# Chapter 4. Effect of external electric fields on recrystallization, grain growth and removal of island grains during annealing in metallic materials

## 4.1 Introduction

In general, a microstructure of metallic materials is controlled by experimental variables such as composition of alloy, temperature and time when the metallic materials are undergone annealing. Recently, as a new possibility for controlling microstructure of metals, an effect of an external electric field on the microstructures in metallic material has been investigated by many researchers. It has been reported that applying the external electric field to bulk metallic materials during annealing affects phenomena related with physical metallurgy such as recrystallization texture [112-115], solution treatment [116-118], phase transformation [119] and segregation of solute atoms [120].

While the effect of the external electric field were investigated in various physical metallurgic phenomena, there are few reports about the effect of the external electric field on recrystallization and grain growth in metallic materials. Some of studies [113, 121, 122] dealt with the effect of the external electric field on recrystallization

and grain growth, but the investigation on pure iron and Fe-base alloys which are representative metallic materials has not been done. Furthermore, it was difficult to clarify the effect of the external electric field on recrystallization and grain growth respectively because annealing procedure in their studies included both stage of recrystallization and grain growth all together. In order to find the effect of the external electric field on recrystallization and grain growth respectively, the experiments should be performed separately. The purpose of this study is to investigate the effect of the external electric field separately on recrystallization and on grain growth in pure iron and Fe-2.9%Si alloy.

Abnormal grain growth, which is also called discontinuous grain growth or secondary recrystallization, has been reported in Fe-3%Si steel and Al 5052 alloy after the heat treatment of deformed polycrystals. One of the distinctive microstructural features in abnormal grain growth is a number of island grains remaining inside abnormally grown grains [123]. In Fe-3%Si steel, which is used for grain oriented electrical steel, it is known that eliminating of the island grains is very important because they deteriorate a magnetic properties [124]. In general, high temperature annealing should be performed for a long time to remove these island grains, which leads to the low productivity. Because the removal behavior of island grains can be categorized in grain growth, it is worth investigating the effect of the external electric field on this behavior as well as grain growth. If the external electric field affect the elimination rate of island grains, it is possible to suggest that the external electric field can be used for application to industrial process for reducing annealing time. In this point of view, Fe-3%Si steel and Al 5052 alloy was also investigated with regard to the effect of the external electric field on a removal of

island grains inside abnormally grown grains during annealing in this chapter.

## 4.2 Experimental procedure

### 4.2.1 The effect of the external electric field on recrystallization

The cold-rolled sheet of high purity iron (99.995 %, Puratronic®) which had thickness of 250 μm was used in this study. For Fe-2.9%Si alloy, an ingot was used as a starting material which had composition of 2.9 Si, 0.45 Al, 0.2 Mn (wt %). The ingot was hot rolled to 2.3mm and followed by cold rolling to 300 μm thickness. The cold rolled sheets of pure iron and Fe-2.9%Si alloy were cut to 35 mm × 15 mm size with rolling direction to be parallel to longitudinal direction of specimens.

The experimental set up for annealing with the external electric field is illustrated in Fig. 4.1. The configuration to apply the external electric field during annealing was similar with reports elsewhere [114, 115]. Specimen was placed between two parallel stainless plates which were 20 mm apart, then specimen and stainless steel plates were electrically connected to anode and cathode of power source, respectively.

To investigate the effect of the external electric field on recrystallization, the cold-rolled specimens of pure iron were subjected to isothermal annealing at 500, 600, 700 and 800 °C for 1 min with and without the external dc electric field of 4 kV/cm. Isothermal annealing was done through moving the specimens from outside to center of a furnace after the furnace temperature had reached the annealing temperature. In the same manner, isothermal annealing was performed for the cold-rolled specimens of Fe-2.9%Si alloy at 650, 700, 750 and 800 °C for 5 min with and without the external electric field of 4 kV/cm. After annealing, the specimens were extracted to

outside of furnace and cooled to room temperature. The annealing treatments were done in a $N_2$ (99.9999 %) atmosphere.

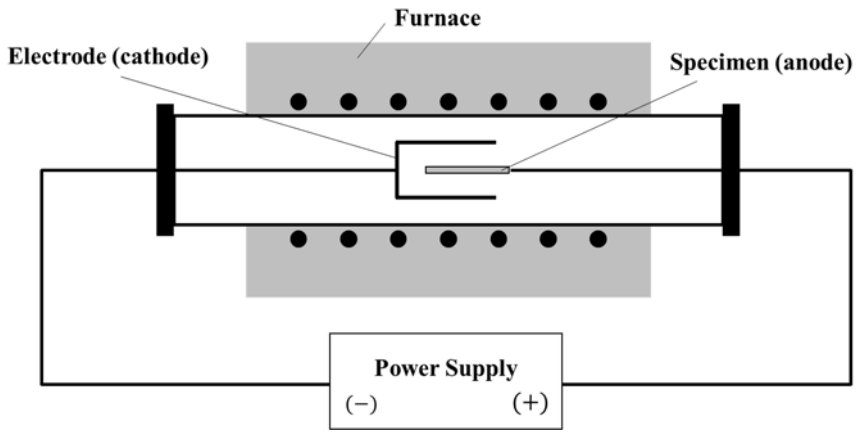


**Fig. 4.1.** The experimental configuration for annealing with and without the external electric field.

In order to observe the microstructures of cross-section, the annealed specimens were sectioned and were chemically etched with 2 % nital solution (98 % ethanol+ 2 % nitric acid) after grinding and polishing. The microstructures were observed using optical microscope (Eclipse L150, Nikon). Vickers hardness specimens were also measured under a load of 1 kgf for 10 sec.

4.2.2 The effect of the external electric field on grain growth

Another experiment was performed to observe the grain growth behavior during annealing with and without the external electric field. It is generally known that recovery, recrystallization and grain growth occur in sequence when cold-worked

metals undergo isothermal annealing [110]. In order to investigate the effects of electric field on grain growth obviously, an initial state of specimen must be in fully recrystallized state. Therefore, pure iron was annealed preferentially at 800 °C for 20 sec to complete recrystallization. After recrystallization, it was annealed at the same temperature for 40 sec with and without the external dc electric field of 4 kV/cm. Similarly, Fe-2.9%Si alloy was annealed at 900 °C for 30 sec to produce completely recrystallized specimen and was further annealed for 150 sec with and without the external dc electric field of 4 kV/cm. The specimen was extracted to outside of furnace and cooled to room temperature after annealing. The annealing treatments were done in a $N_2$ (99.9999 %) atmosphere and the annealing temperature was determined in order to anneal samples in α phase region and not include γ-α phase transformation. The microstructures of cross sections for the specimens annealed were observed using optical microscope after grinding, polishing and chemical etching with 2% nital solution. For the comparison of grain growth behavior between annealing with and without the external electric field, the average grain size of specimen was determined by the Heyn's method [125] which is one of common methods to measure the average grain size. For the statistical reliability, the area of cross section plane was analyzed entirely for the measurement of the average grain size.

4.2.3 The effect of the external electric field on removal of island grains inside abnormally grown grains.

An ingot of Fe-3%Si steel which contains aluminum nitride as an inhibitor to

manufacture the grain oriented electrical steel was hot rolled and cold rolled to 0.3 mm thickness. After primary recrystallization, the steel sheets were heated up to 1100 °C at 5 °C/min, held 30 min and cooled to room temperature to produce a microstructure which shows island grains in inside abnormally grown grains. In order to investigate the elimination rate of the island grains in Fe-3%Si steel during annealing, the specimens were subjected to isothermal annealing at 1100 °C for 5 h and 10 h with and without the external electric field of 2.8 kV/cm. After isothermal annealing with and without the external electric field, the specimens were analyzed using electron backscatter diffraction (EBSD) to measure the fraction of the island grains.

For the specimen of aluminum 5052 alloy, a commercial hot strip having 6mm thickness was cold-rolled to thickness of 1.2 mm. Then, the specimens were underwent primary recrystallization at 400 °C for 1 h. To produce the microstructure showing island grains inside abnormally grown grains, recrystallized specimens were annealed at 530 °C for 2 h. In case of aluminum 5052 alloy, we could trace the sequential microstructure evolution during annealing because of the fact that the aluminum alloy is resistant to oxidation and EBSD measurement can be performed without polishing and etching after a series of sequential annealing [94]. Motivated by this fact, we tried to make ex situ EBSD analysis and measure the fraction of island grains at same area after isothermal annealing at 570 °C for 5 h and 10 h with and without the external electric field of 2.8 kV/cm in order to observe the elimination behavior of island grains in abnormally grown grains.

## 4.3 The effect of the external electric field on recrystallization

The microstructures of pure iron specimen after annealing at 500, 600, 700 and 800 °C for 1 min with and without electric field of 4 kV/cm are shown in Fig. 4.2 and Fig. 4.3. The specimens annealed at 500 °C show the microstructure of cold-rolled state, which means that the specimens were not recrystallized in both specimens annealed with and without the external electric field. Recrystallization starts at 600 °C as shown in Fig. 4.2(b) and 4.3(b). At 600 °C, it is observed that recrystallization proceeded much more in the specimens annealed with the external electric field than the specimens annealed without the external electric field. In other words, the rate of recrystallization was enhanced by the external electric field. The specimens annealed at 700 °C and 800 °C are fully recrystallized. However, in case of annealing at 800 °C, the grain size of the specimen annealed with the external electric field is larger than that of the specimen annealed conventionally as shown Fig. 4.2(d) and 4.3(d). It seems that the grain growth rate was enhanced by the external electric field at the stage of grain growth after recrystallization, which will be discussed later.

Fig. 4.4 and Fig. 4.5 show the microstructures of Fe-2.9%Si alloy specimen after annealing at 650, 700, 750 and 800 °C for 5 min with and without electric field of 4 kV/cm. Both of the specimens annealed with and without the electric field are partially recrystallized when they were annealed at 650 and 700 °C for 5 min as shown in Fig. 4.4(a), 4.4(b), 4.5(a) and 4.5(b). When the specimens were annealed at 750 and 800 °C, both of them annealed with and without the external electric field shows the microstructure of the specimen which were fully recrystallized. In Fe-

2.9%Si alloy, however, it was difficult to compare the difference obviously between the specimens annealed with and without the external electric field. Therefore, these specimens were further analyzed by EBSD to measure a fraction of recrystallization. The fraction of recrystallization of the specimens was determined by calculating grain orientation spread (GOS) value of grains which is common criterion for the measurement of recrystallization fraction [126, 127]. The grains which have the GOS value below 0.5° are considered as recrystallized grains and their fraction was measured for the Fe-2.9%Si alloy specimens annealed with and without the external electric field at each annealing temperature. The recrystallized fraction of annealed specimen is listed in Table 4.1. The specimens annealed with the external electric field were recrystallized more than those annealed conventionally as listed in Table 4.1, which means that the external electric field also enhanced recrystallization process in Fe-2.9%Si alloy.

Fig. 4.6 shows the Vickers hardness of specimens after annealing with and without the external electric field of 4 kV/cm in pure iron and Fe-2.9%Si alloy. It is observed that the hardness of the specimens annealed with the external electric field was lower than that of the specimens annealed without the external electric field. The hardness results imply that the rate of recrystallization was enhanced by the external electric field during annealing in pure iron and Fe-2.9%Si alloy.

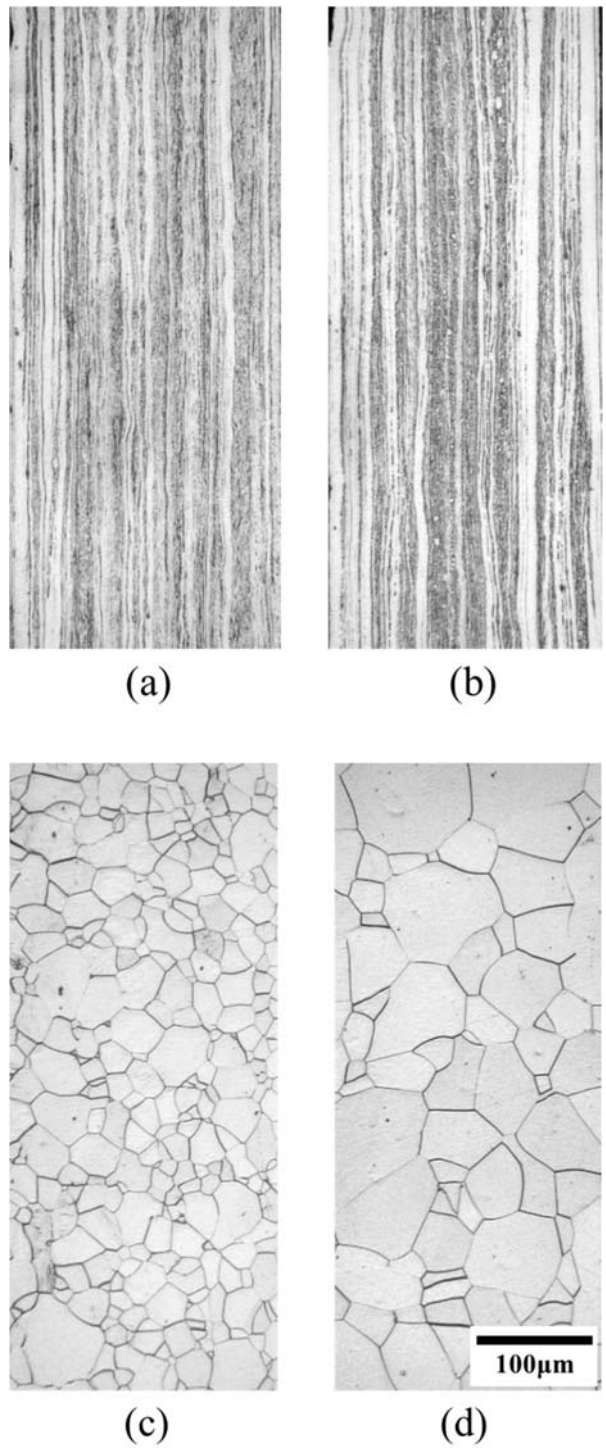


**Fig. 4.2.** The microstructures of pure iron specimens annealed without the external electric field at (a) 500 °C, (b) 600 °C, (c) 700 °C and (d) 800 °C.

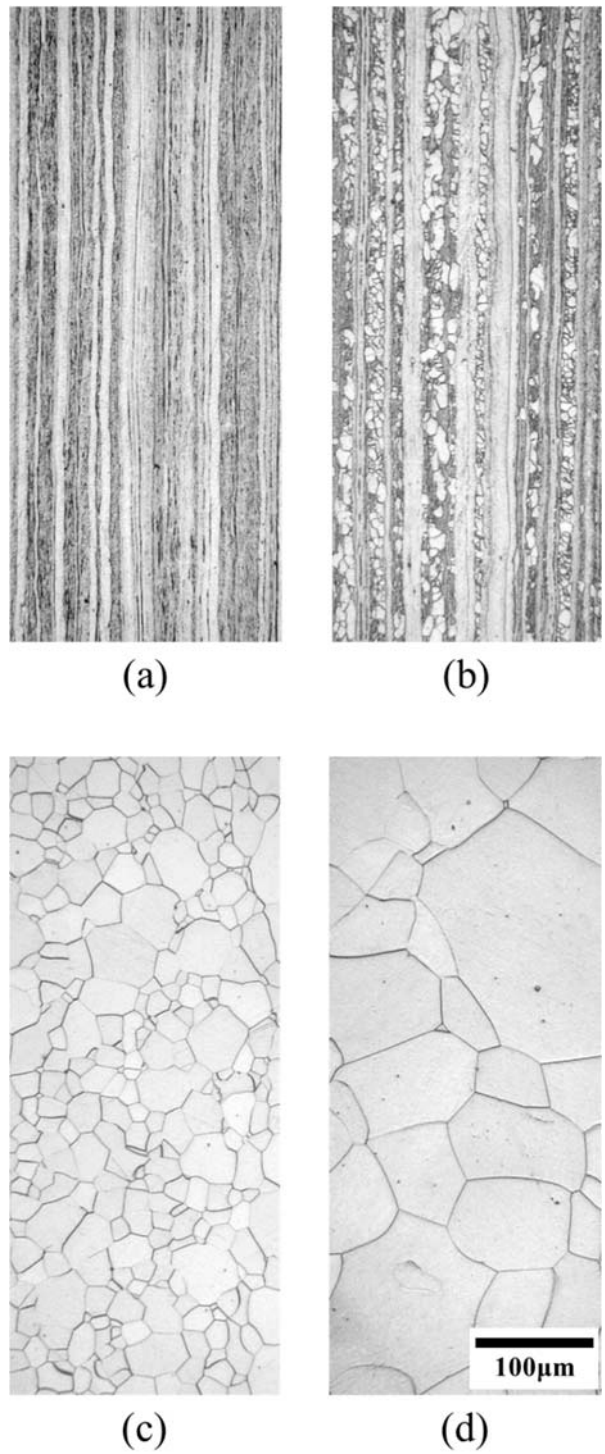


**Fig. 4.3.** The microstructures of pure iron specimens annealed with the external electric field of 4 kV/cm at (a) 500 °C, (b) 600 °C, (c) 700 °C and (d) 800 °C.

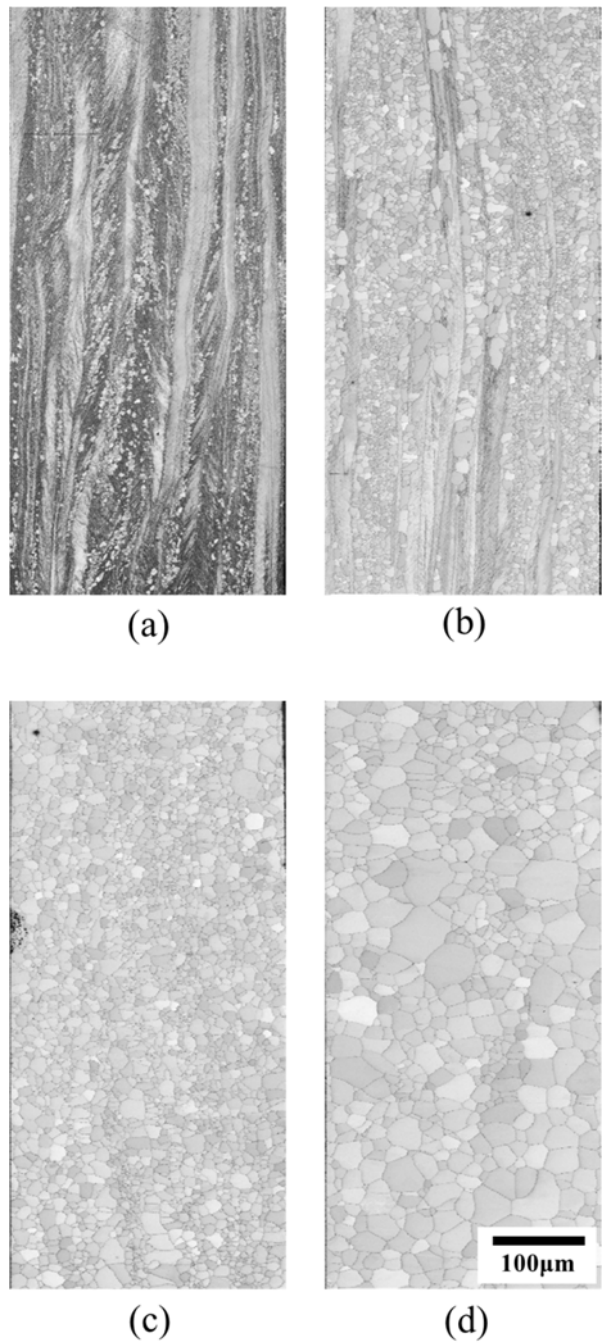


**Fig. 4.4.** The microstructures of Fe-2.9%Si alloy specimens annealed without the external electric field at (a) 650 °C, (b) 700 °C, (c) 750 °C and (d) 800 °C.

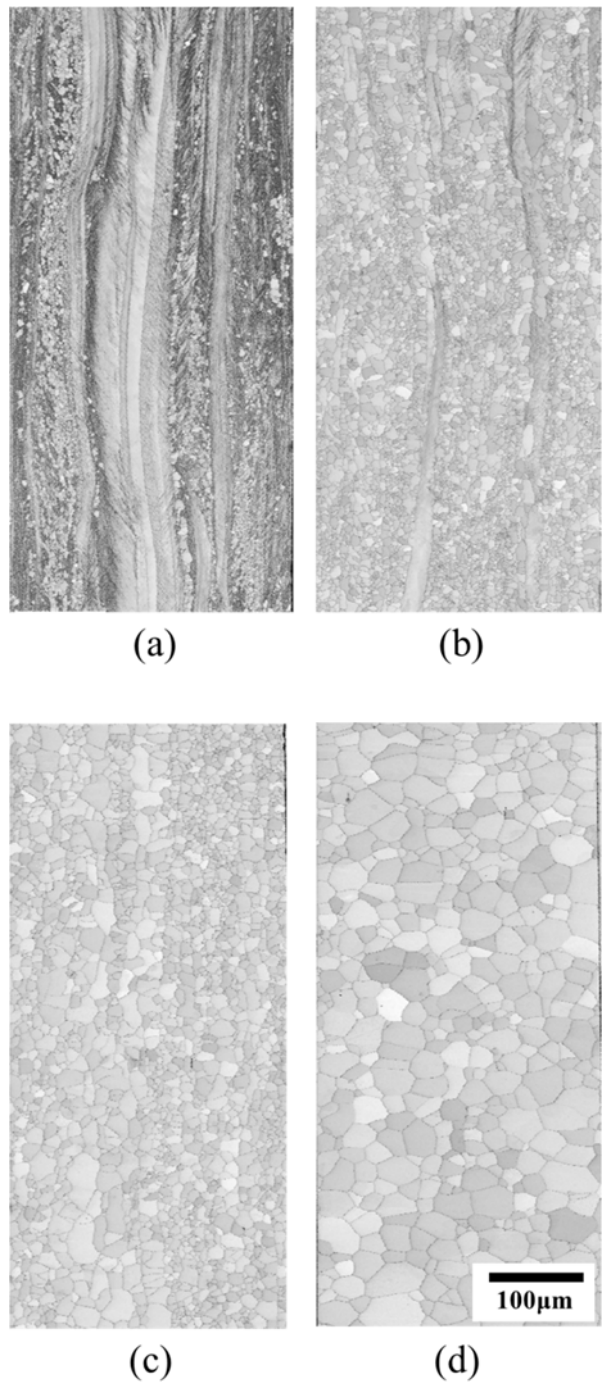


**Fig. 4.5.** The microstructures of Fe-2.9%Si alloy specimens annealed with the external electric field of 4 kV/cm at (a) 650 °C, (b) 700 °C, (c) 750 °C and (d) 800 °C.

| Annealing temperature °C | Annealing time (min) | Recrystallized fraction (%) | |
|---|---|---|---|
| | | Without the external electric field | With the external electric field |
| 650 | 5 | 15.9 | 22 |
| 700 | | 59.4 | 69.2 |
| 750 | | 77.1 | 79.7 |
| 800 | | 96.3 | 96 |

**Table 4.1.** Recrystallized fraction of the specimen annealed with and without the external electric field at each annealing temperature in Fe-2.9%Si alloy.

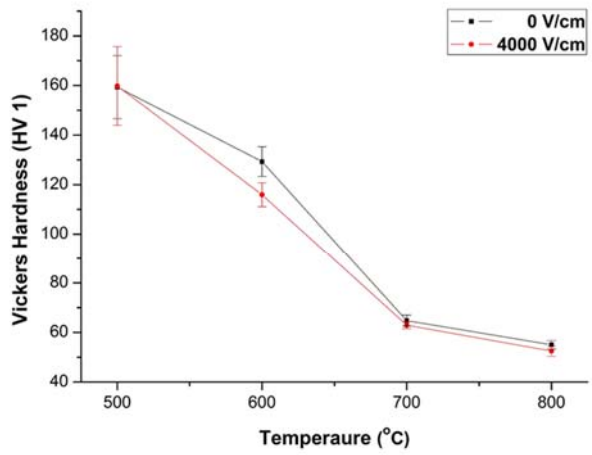


(a)

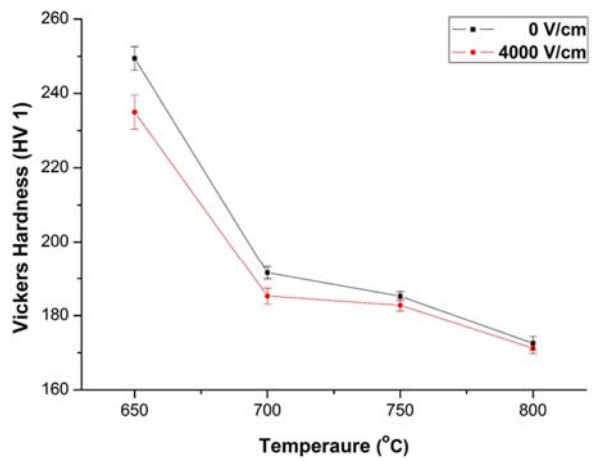


(b)

**Fig. 4.6.** The Vickers hardness of specimens after annealing with and without the external electric field of 4 kV/cm in (a) pure iron and (b) Fe-2.9%Si alloy.

## 4.4 The effect of the external electric field on grain growth

It is observed that pure iron specimen annealed preferentially at 800 °C for 20 sec was recrystallized completely as shown in Fig. 4.7(a). Thus, it can be considered that the microstructure evolution during subsequent annealing at 800 °C for 40 sec with or without the external electric field is entirely governed by grain growth. Recrystallized pure iron specimen after annealing at 800 °C for 20 sec had the average grain size of 25.68 μm. Fig. 4.7(b) and 4.7(c) show the microstructures evolved after subsequent annealing at 800 °C for 40 sec without and with the external electric field respectively. Although grain growth occurred in both of the specimens, the difference in the grain size between specimens annealed with and without the external electric field was remarkably large as shown in Fig. 4.7(a) and 4.7(b). The average grain size was 52.12 μm for the specimen after conventional annealing, while it was 98.89 μm for the specimen after annealing with the external electric field.

In Fe-2.9%Si alloy, the tendency of grain growth behavior concerned with the effect of the external electric field was similar with the case of pure iron as shown in Fig. 4.8. Fig. 4.8(a) shows that the cold-rolled sheet of Fe-2.9%Si alloy was completely recrystallized after annealing at 900 °C for 30 sec. The average grain size of the recrystallized state of specimen after annealing for 30 sec at 900 °C was 18.92 μm. When this recrystallized specimen was further annealed for 150 sec with electric field, the specimen shows much larger grain size than that annealed for 150 sec without electric field as shown in Fig. 4.8(b) and 4.8(c). The average grain size of the specimen was 58.05 μm and 103.14 μm for the specimen annealed without and

with the external electric field, respectively.

The ratios of the average grain size of the specimen annealed with external electric field of 4 kV/cm to that of the specimen annealed conventionally were 1.89 and 1.78 for pure iron and Fe-2.9%Si alloy respectively, which implies that the grain growth rate during annealing with the external electric field was almost twice as high as that during conventional annealing.

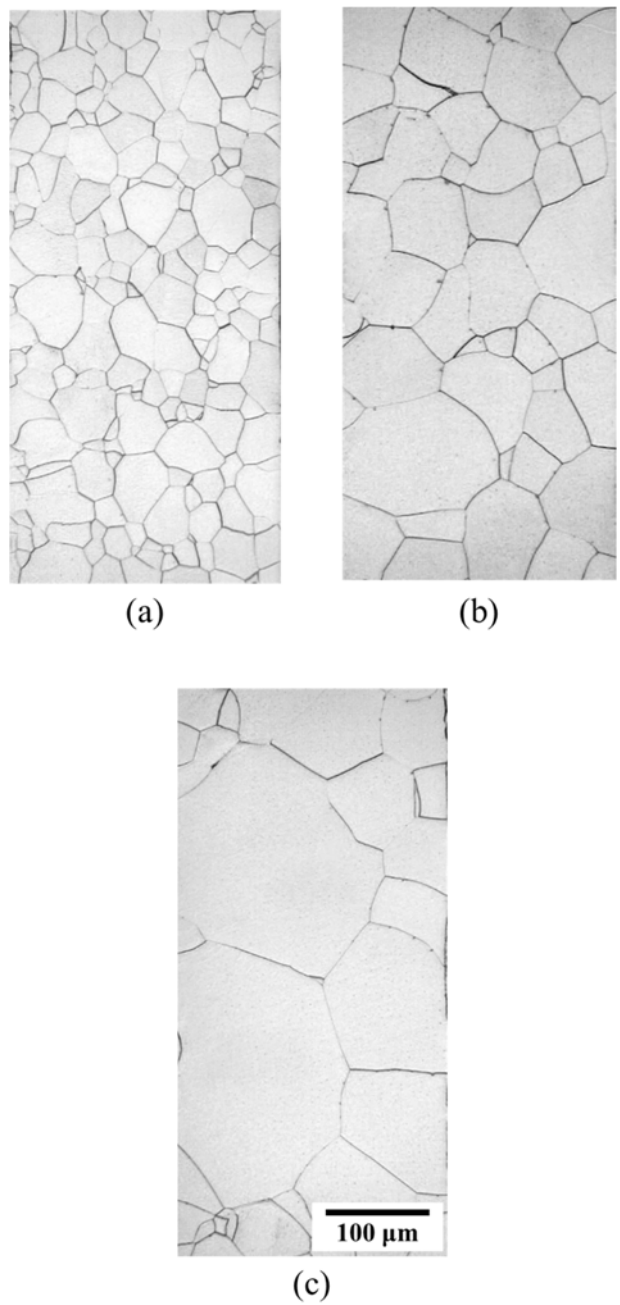


**Fig. 4.7.** Microstructures of pure iron specimens after (a) recrystallization (annealed at 800 °C for 20 sec), (b) annealing at 800 °C 40 sec without the external electric field and (c) annealing at 800 °C 40 sec with the external electric field of 4 kV/cm.

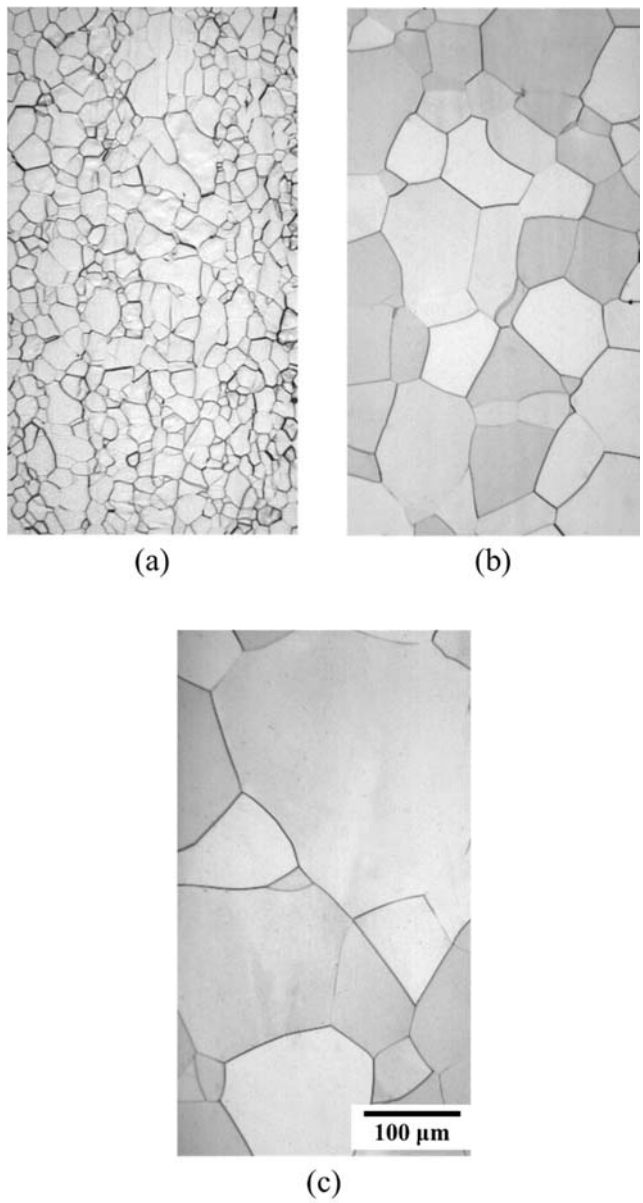


**Fig. 4.8.** Microstructures of Fe-2.9%Si alloy specimens after (a) recrystallization (annealed at 900 °C for 30 sec), (b) annealing at 900 °C 150 sec without the external electric field and (c) annealing at 900 °C 150 sec with the external electric field of 4 kV/cm.

## 4.5 The effect of the external electric field on removal of island grains inside abnormally grown grains

Fig. 4.9(a) show the microstructure of specimen of Fe-3%Si steel which was heated up to 1100 °C at 5 °C/min and held 30 min which is the initial state of experiment. The island grains exist inside Goss grains. Using filtering tool which is included in EBSD software (TSL OIM), the island grains is extracted to measure the fraction of island grains as shown Fig. 4.9(b). Similarly, the IPF map and filtered IPF map after annealing for 5 h and 10 h at 1100 °C with and without the external electric field of 2.8 kV/cm are shown in Fig. 4.10 and 4.11 respectively.

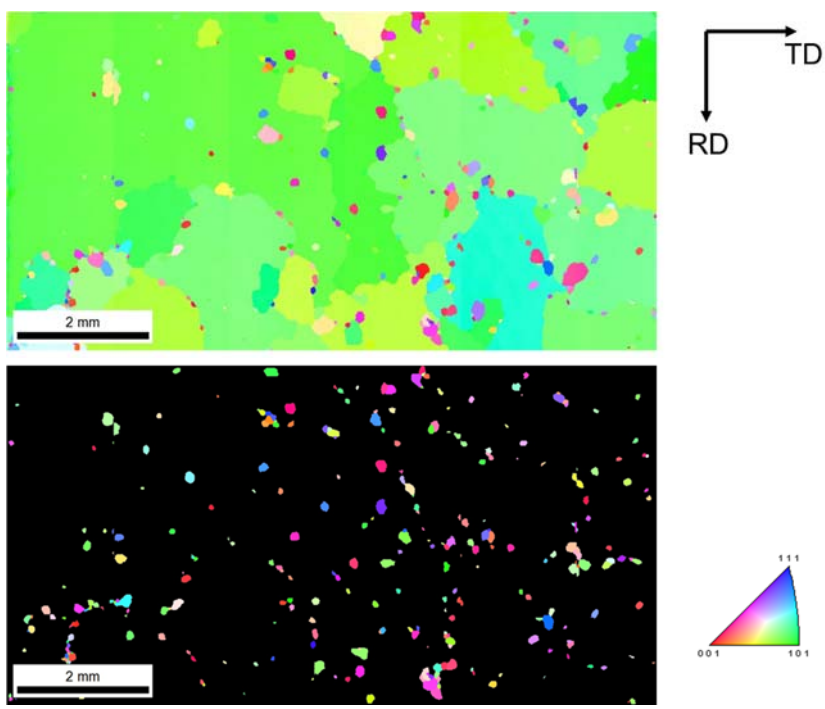


**Fig. 4.9.** (a) IPF map of specimens of Fe-3%Si steel at initial state ( specimen heated up to 1100 °C at 5 °C/min and held 30 min) (b) IPF map after filtering grains except the island grains.

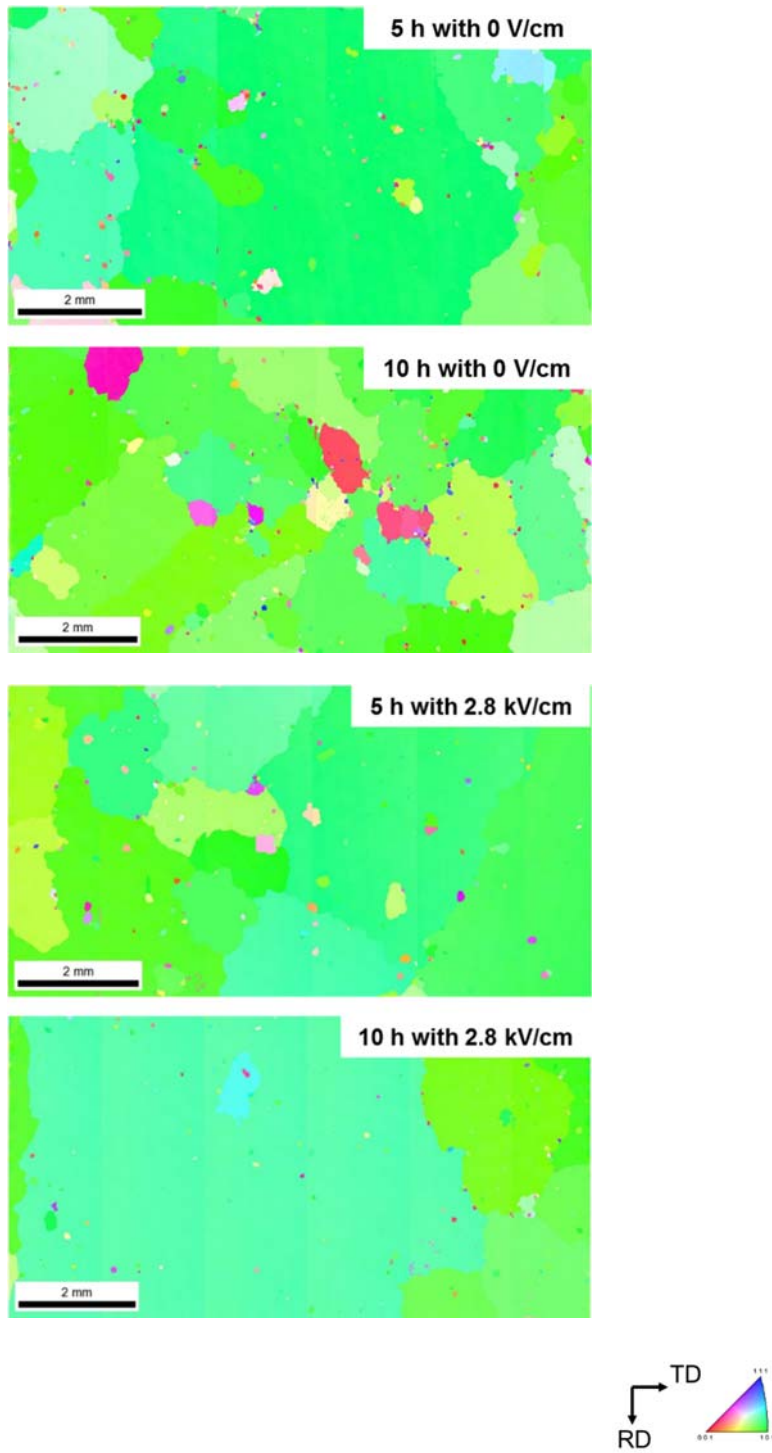


**Fig. 4.10.** IPF map of specimens which annealed for 5 h and 10 h at 1100 °C with and without the external electric field.

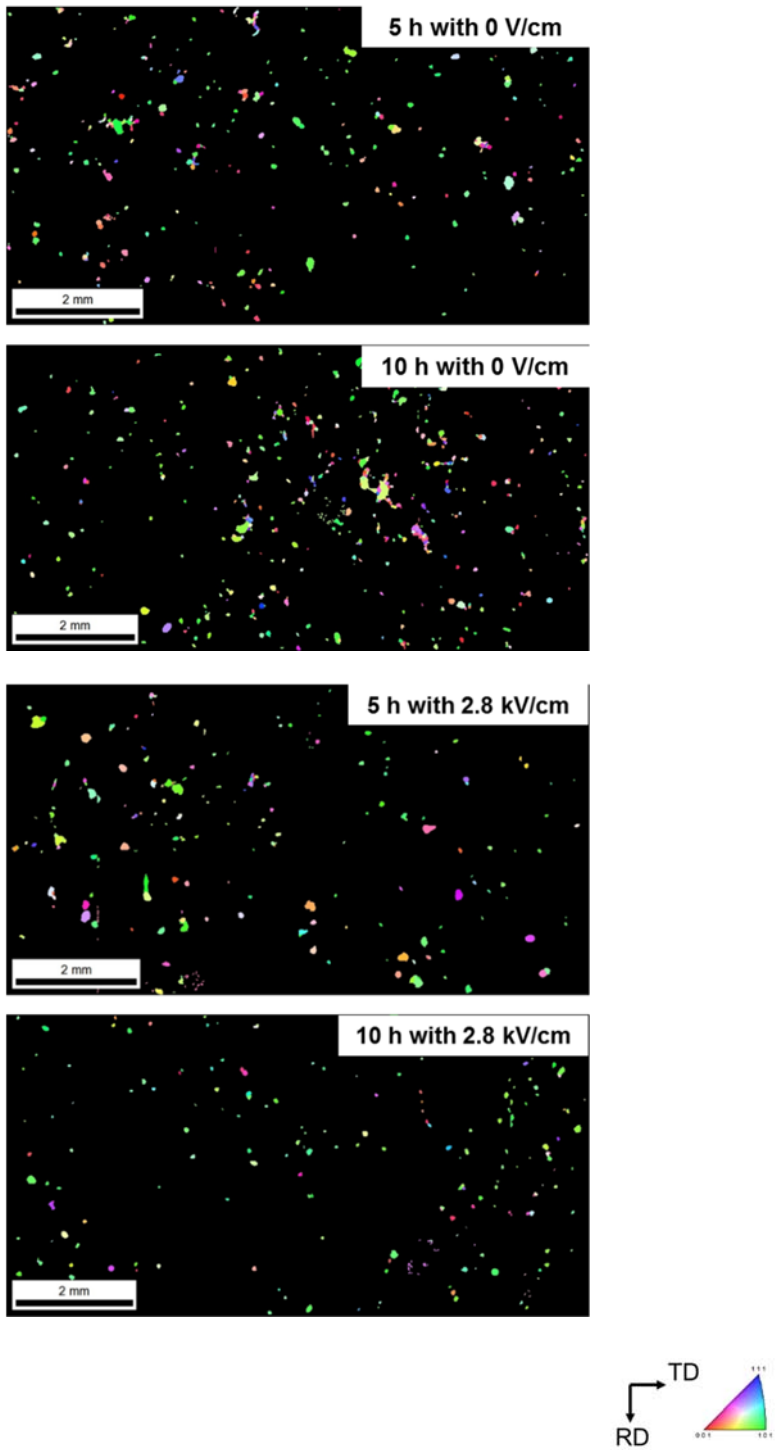


**Fig. 4.11.** IPF map of specimens which annealed for 5 h and 10 h at 1100 °C with and without the external electric field after filtering grains except island grains.

As to Al 5052 alloy, the microstructures of specimen of Al 5052 alloy which are the initial state of experiment are shown in Fig. 4.12. The specimens in Fig 4.12 were annealed for 5 and 10 h at 570 °C with and without the external electric field of 2.8 kV/cm, and the island grain maps for each annealing condition are shown in Fig 4.13.

Fig. 4.14 shows the fraction of island grains inside abnormally grown grains after annealing with and without the external electric field in Fe-3%Si steel and Al 5052 alloy. In Fe-3%Si steel, the fraction of island grains was reduced from 3.3 % to 2.1 % after annealing for 5 hours, but the fraction was not decreased any more until 10 hours for annealing when the specimens were annealed without the external electric field. However, the fraction of island grains decreased consistently from 3.3 % to 1.3 % after annealing for 10 hours when the specimens were annealed with the external electric field of 2.8 kV/cm as shown in Fig. 4.14(a). In Al 5052 alloy, which were analyzed by ex situ EBSD measurement at same area, similar behavior was observed. The fraction of island grains decreased more rapidly during annealing with the external electric field of 2.8 kV/cm (from 3.2 % to 1.1 %) than during annealing without the external electric field (from 3.1 % to 2.0 %) as shown Fig. 4.14(b). The decreasing rates of island grains increased by 1.67 times and 1.9 times in Fe-3%Si steel and Al 5052 alloy respectively when the external electric field was applied during annealing, which means that the elimination of island grains inside abnormally grown grains was accelerated by the external electric field.

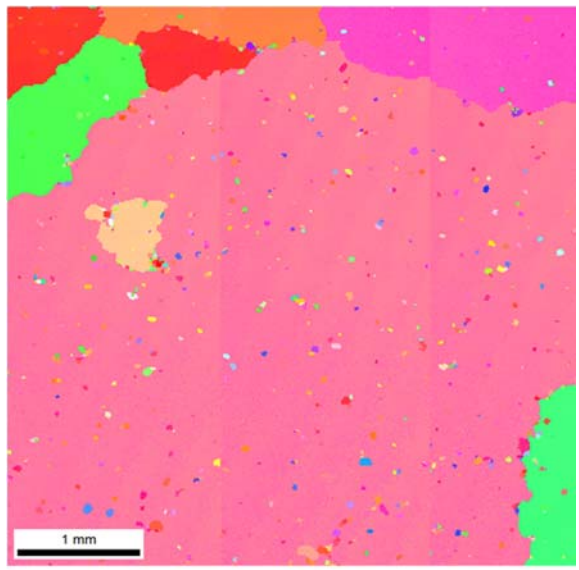


(a)

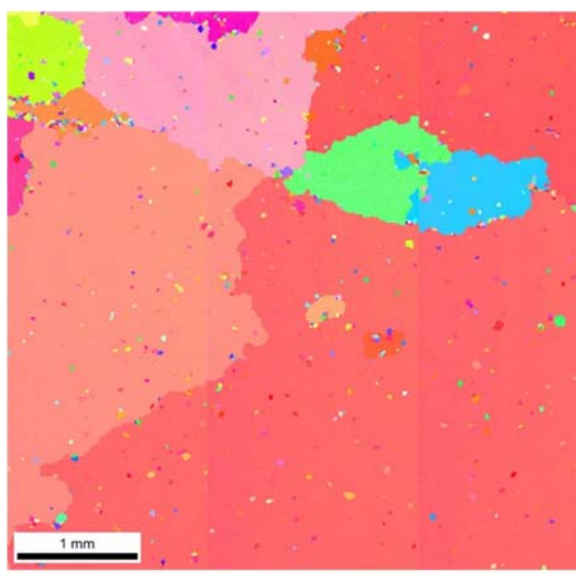


(b)

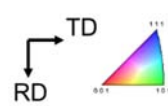


**Fig. 4.12.** IPF map of specimens of Al 5052 alloy at initial state (specimens annealed at 530 °C for 2h) for annealing (a) without the external electric field (b) with the external electric field of 2.8 kV/cm.

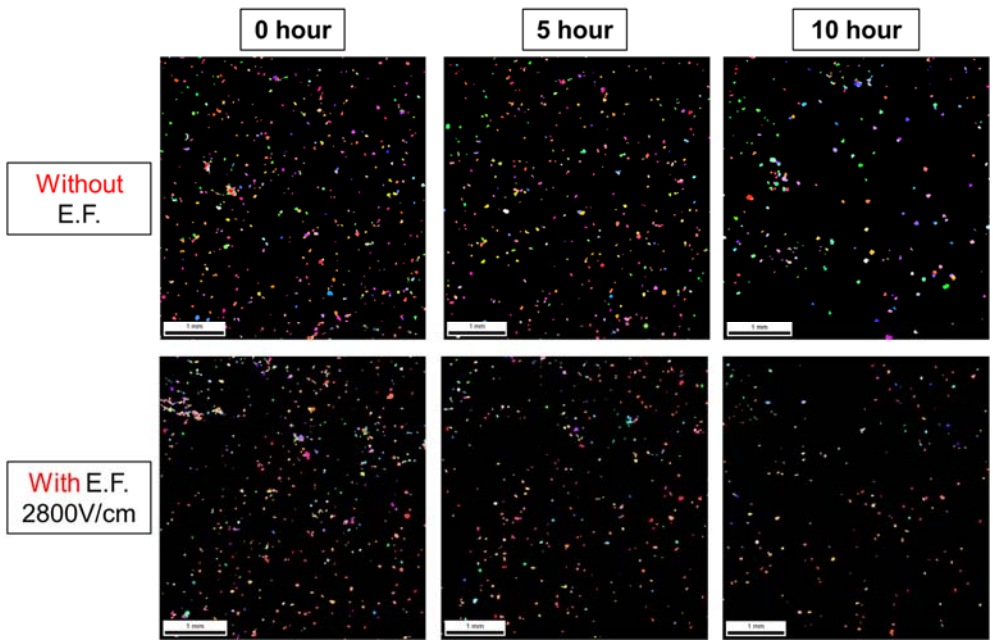


**Fig. 4.13.** IPF map of specimens which annealed for 5 h and 10 h at 570 °C with and without the external electric field after filtering grains except island grains.

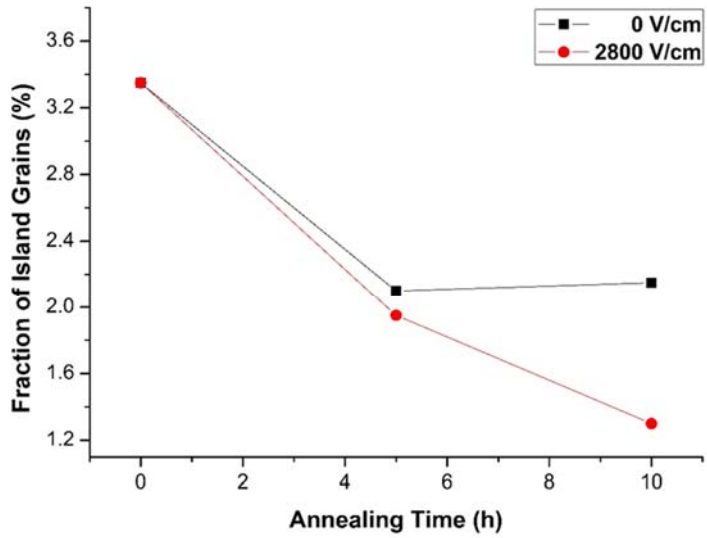


(a)

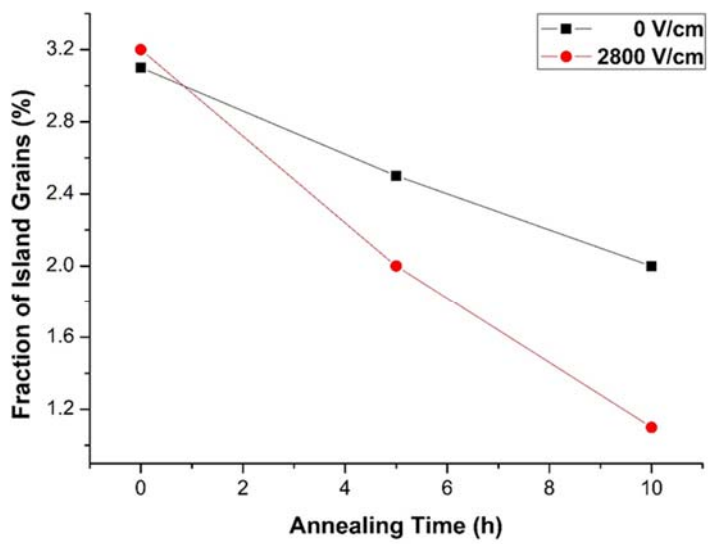


(b)

**Fig. 4.14.** The fraction of island grains after annealing with and without the external electric field in (a) Fe-3%Si steel and (b) Al 5052 alloy.

## 4.6 The effect of the external electric fields focusing on the acceleration of the rate of recrystallization and grain growth in metals

According to the results in this study, it can be said that applying the external electric field enhances the kinetics of recrystallization and grain growth during annealing.

On the effect of the external electric field on recrystallization, there were some reports that suggested the retardation of recrystallization by the external electric field during annealing. Some researchers [113, 122] suggested that the external electric field might perturb the crystal defects in bulk metals and contribute to change behavior of recrystallization, but detail explanation was not made. Yan et al. [112] reported the retardation effect of the external electric field in aluminum sheet and proposed that the crystal defects such as vacancy, dislocation, grain boundary which play an important role as a nucleation site at initial stage of recrystallization move out to surface by the external electric field. However, in their studies, the difference of hardness between the specimens annealed with and without the external electric field were not significant when their mechanism is considered. So it can be considered that underlying mechanism associated with the effects of the external electric field on recrystallization is not fully understood.

On the other hand, the similar results related to the effect of the external electric field on grain growth were reported in other systems of ceramic and metallic films. Jin et al. [128] observed grain growth behavior of polycrystalline barium titanate ($BaTiO_3$) and reported that grain growth was enhanced during annealing with the

external electric field. Li et al. [129] also reported enhanced grain growth by external electric field during annealing of $La_2Ti_2O_7$ ferroelectric thin films deposited by method of chemical solution deposition. In addition to ceramic system, large grains were observed after annealing with applying the external electric field in nanocrystalline copper films by Cao et al. [130]. However, mechanism for the effects of the external electric field on grain growth has not been fully understood so far.

In metallic materials, it is generally known that the excess charges are induced only at surface and there is no excess charge interior of metal when the external electric field is applied to bulk metals. However, the experimental results showed that microstructure was affected by the external electric field not only at surface region but also at interior of samples because the accelerating phenomena were also observed at interior of specimens.

One of possibilities for the effect of the external electric field is that the external field might raise a temperature of the specimens. In order to investigate the effect of the external effect on the temperature of the specimens, additional experiment was done. Thermocouple was attached to the specimens to measure the temperature of specimens and the specimens were subjected to the isothermal annealing of 900 °C with and without the external electric field. As a result, the temperature difference between specimens annealed with and without the external electric field was about 0.4 °C, which is very small. Thus it can be said that the effect of the external electric field on the temperature of specimens are negligible.

Metals generally have defects such as vacancy, dislocation and grain boundary. It can be suggested that the interior of the specimens could be affected by the external electric field because surface charges induced by the external electric field could

have influence on the crystal defects.

According to the electron theory of metals, it is considered that the lattice defects including vacancy, dislocation and grain boundary are relatively electronegative because of absence of positive metallic ions [131]. Electric charge at surface of metals induced by the external electric field could affect the electric state of these defects in interior of metals [120]. It can be suggested that the energy state of the crystal defects which are locally electronegative and the atoms near these defects could be excited because they get an additional electrostatic energy by surface charge induced by the external electric field. Therefore, the excited defects including vacancy, dislocation and atoms neighboring these defects could easily overcome an activation energies for nucleation of defect-free nuclei and there by the rate recrystallization is enhanced when the cold-rolled metals undergo annealing for recrystallization with the external electric field.

The explanation for the effect of the external electric field, which is suggested above, can be also applied to the acceleration of the grain growth and the elimination of island grains as well as recrystallization. The grain growth and the removal of island grains are generally accompanied by the migration of the grain boundary. In atomistic view, the migration of grain boundary is the migration of atoms including atomic jump across the grain boundary. In other words, the velocity of the grain boundary migration is proportional to the rate of atomic jump across the grain boundary [132]. Because the energy state of the crystal defects such as grain boundary and neighboring atoms could be excited by the external electric field, as explained above, atoms near the grain boundary could easily overcome the activation energy for the migration of atom across the grain boundary. Thus, the grain growth

and the elimination of island grain which were accompanied by migration of grain boundary could be accelerated by the external electric field.

# Chapter 5. Conclusion

It is revealed by synchrotron X-ray microdiffraction that abnormally-growing Goss grains selectively have sub-boundaries of which misorientation angle is extremely low in Fe-3wt%Si steel. This result agrees with the previous literatures correlating between AGG and sub-boundaries and implies that the sub-boundaries should play an important role in AGG of Goss grains in Fe-3wt%Si steel.

Also, in relation to the mechanism of sub-boundary enhanced solid state wetting and the facts that sub-boundary exist in abnormally growing Goss grains in Fe-3%Si steel, abnormal grain growth of non-Goss grains was induced by forming sub-boundary through low deformation in Fe-3%Si steel.

It is observed that the kinetics of recrystallization and grain growth was accelerated by applying the external electric field during annealing in pure iron and Fe-2.9%Si alloy. The elimination of the island grains inside abnormally grown grains was also accelerated by the external electric field during annealing in Fe-3%Si steel and Al 5052 alloy. Considering the effects of the external electric field on metallic materials, it is suggested that the activation energies for the recrystallization and the migration of grain boundary could be easily overcome by the external electric field because the excess electric charges at surface of metal induced by the external electric field could excite the energy state of the crystal defects and nearby atoms.

# Bibliography

[1] M. Hillert, Acta Metall., 13 (1965) 227-238.

[2] T. Omori, T. Kusama, S. Kawata, I. Ohnuma, Y. Sutou, Y. Araki, K. Ishida, R. Kainuma, Science, 341 (2013) 1500-1502.

[3] B. Sarrail, C. Schrupp, S. Babakhanyan, K. Muscare, J. Foyos, J. Ogren, S. Sparkowich, R. Sutherlin, J. Hilty, R. Clark Jr, O.S. Es-Said, Eng. Fail. Anal., 14 (2007) 652-655.

[4] Y.B. Chun, S.K. Hwang, S.I. Kwun, M.H. Kim, Scripta Mater., 40 (1999) 1165-1170.

[5] S.H. Lee, J.S. Choi, D.Y. Yoon, Z. Metallkd., 92 (2001) 655-662.

[6] J.S. Choi, D.Y. Yoon, ISIJ Int., 41 (2001) 478-483.

[7] K.I. Moon, H.S. Park, K.S. Lee, Mater. Sci. Eng., A, 323 (2002) 293-300.

[8] S.B. Lee, N.M. Hwang, D.Y. Yoon, M.F. Henry, Metall. Mater. Trans. A, 31 (2000) 985-994.

[9] R. Messina, M. Soucail, T. Baudin, L.P. Kubin, J. Appl. Phys., 84 (1998) 6366-6371.

[10] J. Dennis, P.S. Bate, F.J. Humphreys, Acta Mater., 57 (2009) 4539-4547.

[11] H.C. Kim, C.G. Kang, M.Y. Huh, O. Engler, Scripta Mater., 57 (2007) 325-327.

[12] H.G. Suk, E.J. Shin, M.Y. Huh, Solid State Phenom., 2006, pp. 316-319.

[13] D.W. Suh, S.Y. Lee, K.H. Lee, S.K. Lim, K.H. Oh, J. Mater. Process. Technol., 155-156 (2004) 1330-1336.

[14] P.R. Rios, G. Gottstein, Acta Mater., 49 (2001) 2511-2518.

[15] H. Park, D.N. Lee, J. Mater. Process. Technol., 113 (2001) 551-555.

[16] N.A. Pedrazas, T.E. Buchheit, E.A. Holm, E.M. Taleff, Mater. Sci. Eng., A, 610 (2014) 76-84.

[17] D.L. Worthington, N.A. Pedrazas, P.J. Noell, E.M. Taleff, Metall. Mater. Trans. A, 44 (2013) 5025-5038.

[18] K. Jae Bon, Y. Duk Yong, Metall. Mater. Trans. A, 32 (2001) 1911-1926.

[19] J.B. Koo, D.Y. Yoon, M.F. Henry, Metall. Mater. Trans. A, 31 (2000) 1489-1491.

[20] B.B. Straumal, W. Gust, V.G. Sursaeva, V.N. Semenov, L.S. Shvindlerman, in: Mater. Sci. Forum, 1999, pp. 533-536.

[21] F. Ma, J.M. Zhang, K.W. Xu, Appl. Surf. Sci., 242 (2005) 55-61.

[22] J. Greiser, P. Müllner, E. Arzt, Acta Mater., 49 (2001) 1041-1050.

[23] H.-J. Lee, H.N. Han, D.H. Kim, U.-h. Lee, K.H. Oh, P.-R. Cha, Appl. Phys. Lett., 89 (2006) -.

[24] V. Weihnacht, W. Brückner, Thin Solid Films, 418 (2002) 136-144.

[25] J.M. Zhang, K.W. Xu, V. Ji, J. Cryst. Growth, 226 (2001) 168-174.

[26] U. Klement, M. da Silva, J. Alloys Compd., 434-435 (2007) 714-717.

[27] O. Arnould, O. Hubert, F. Hild, in: Mater. Sci. Forum, 2004, pp. 957-962.

[28] K. Harada, S. Tsurekawa, T. Watanabe, G. Palumbo, Scripta Mater., 49 (2003) 367-372.

[29] K.I. Moon, K.S. Lee, J. Alloys Compd., 333 (2002) 249-259.

[30] J. Greiser, D. Müller, P. Müllner, C.V. Thompson, E. Arzt, Scripta Mater., 41 (1999) 709-714.

[31] B.D. Cullity, C.D. Graham, Introduction to Magnetic Materials, Wiley, 2009.

[32] S.B. Lee, N.M. Hwang, C.H. Han, D.Y. Yoon, Scripta Mater., 39 (1998) 825-829.

[33] J.T. Park, R.E. Park, J.S. Woo, J. Kor. Inst. Metall. Mater., 32 (1994) 616-624.

[34] N.P. Goss, T. Am. Soc. Metal., 23 (1935).

[35] J.E. May, D. Turnbull, Trans.metall. Soc. AIME 212 (1958) 769-781.

[36] P.R. Rios, Scripta Mater., 38 (1998) 1359-1364.

[37] P.R. Rios, Acta Mater., 45 (1997) 1785-1789.

[38] P.R. Rios, Acta Metall. Mater., 42 (1994) 839-843.

[39] N.C. Pease, D.W. Jones, M.H.L. Wise, W.B. Hutchinson, Met. Sci., 15 (1981) 203-209.

[40] P. Lin, G. Palumbo, J. Harase, K.T. Aust, Acta Mater., 44 (1996) 4677-4683.

[41] N. Chen, S. Zaefferer, L. Lahn, K. Günther, D. Raabe, Acta Mater., 51 (2003) 1755-1765.

[42] Y. Inokuti, C. Maeda, Y. Ito, T. Iron Steel I. Jpn, 27 (1987) 139-144.

[43] J. Harase, R. Shimizu, D.J. Dingley, Acta Metall. Mater., 39 (1991) 763-770.

[44] J. Harase, R. Shimizu, Acta Metall. Mater., 38 (1990) 1395-1403.

[45] R. Shimizu, J. Harase, Acta Metall., 37 (1989) 1241-1249.

[46] Y. Yoshitomi, Y. Ushigami, J. Harase, T. Nakayama, H. Masui, N. Takahashi, Acta Metall. Mater., 42 (1994) 2593-2602.

[47] Y. Yoshitomi, K. Iwayama, T. Nagashima, J. Harase, N. Takahashi, Acta Metall. Mater., 41 (1993) 1577-1585.

[48] Y. Ushigami, Y. Arira, K. Ushioda, in: Mater. Sci. Forum, 2013, pp. 337-340.

[49] Y. Ushigami, S. Nakamura, in: Mater. Sci. Forum, 2012, pp. 122-127.

[50] Y. Ushigami, T. Kumano, T. Haratani, S. Nakamura, S. Takebayashi, T. Kubota, in: B. Bacroix, J.H. Driver, R. Gall, C. Maurice, R. Penelle, H. Regle, L. Tabourot (Eds.), Annecy, 2004, pp. 853-862.

[51] Y. Ushigami, S. Nakamura, S. Takebayashi, S. Suzuki, in: Mater. Sci. Forum, 2002, pp. 973-978.

[52] Y. Ushigami, T. Kubota, N. Takahashi, ISIJ Int., 38 (1998) 553-558.

[53] T. Kumano, T. Haratani, Y. Ushigami, ISIJ Int., 43 (2003) 736-745.

[54] T. Kumano, T. Haratani, Y. Ushigami, ISIJ Int., 42 (2002) 440-449.

[55] H. Homma, K. Murakami, T. Tamaki, N. Shibata, T. Yamamoto, Y. Ikuhara, in: Mater. Sci. Forum, 2007, pp. 633-640.

[56] H. Homma, B. Hutchinson, Acta Mater., 51 (2003) 3795-3805.

[57] B. Hutchinson, in: Mater. Sci. Forum, 2012, pp. 73-80.

[58] N. Maazi, R. Penelle, Mater. Sci. Eng., A, 504 (2009) 135-140.

[59] N. Rajmohan, J.A. Szpunar, Scripta Mater., 44 (2001) 2387-2392.

[60] N. Rajmohan, J.A. Szpunar, Y. Hayakawa, Mater. Sci. Eng., A, 259 (1999) 8-16.

[61] N. Rajmohan, J.A. Szpunar, Y. Hayakawa, Acta Mater., 47 (1999) 2999-3008.

[62] Y. Hayakawa, M. Muraki, J.A. Szpunar, Acta Mater., 46 (1998) 1063-1073.

[63] Y. Hayakawa, J.A. Szpunar, Acta Mater., 45 (1997) 4713-4720.

[64] Y. Hayakawa, J.A. Szpunar, Acta Mater., 45 (1997) 1285-1295.

[65] Y. Hayakawa, J.A. Szpunar, G. Palumbo, P. Lin, J. Magn. Magn. Mater., 160 (1996) 143-144.

[66] H. Park, D.Y. Kim, N.M. Hwang, Y.C. Joo, C.H. Han, J.K. Kim, J. Appl. Phys., 95 (2004) 5515-5521.

[67] J. Harase, R. Shimizu, J.K. Kim, J.S. Woo, Met. Mater. Int., 5 (1999) 429-435.

[68] A.L. Etter, T. Baudin, R. Penelle, in: Mater. Sci. Forum, 2002, pp. 1251-1256.

[69] A.L. Etter, T. Baudin, R. Penelle, Scripta Mater., 47 (2002) 725-730.

[70] A. Morawiec, Scripta Mater., 43 (2000) 275-278.

[71] D. Dorner, L. Lahn, S. Zaefferer, in: Mater. Sci. Forum, 2004, pp. 129-134.

[72] G. Gottstein, L.S. Shvindlerman, B. Zhao, Scripta Mater., 62 (2010) 914-917.

[73] G. Gottstein, Y. Ma, L.S. Shvindlerman, Acta Mater., 53 (2005) 1535-1544.

[74] G. Gottstein, L.S. Shvindlerman, Scripta Metall. Mater., 27 (1992) 1515-1520.

[75] N.M. Hwang, in: B. Bacroix, J.H. Driver, R. Gall, C. Maurice, R. Penelle, H. Regle, L. Tabourot (Eds.), Annecy, 2004, pp. 745-750.

[76] N.M. Hwang, S.B. Lee, D.Y. Kim, Scripta Mater., 44 (2001) 1153-1160.

[77] N.M. Hwang, J. Mater. Sci., 33 (1998) 5625-5629.

[78] N.M. Hwang, D.K. Lee, K.J. Ko, B.J. Lee, J.T. Park, B.D. Hong, J.K. Kim, D.Y. Kim, Alternative mechanism of secondary recrystallization: Solid-state wetting Along grain boundaries or triple junctions, in, Proceedings of an International Conference on Solid-Solid Phase Transformations in Inorganic Materials 2005, 2005, pp. 591-608.

[79] C.S. Park, T.W. Na, H.K. Park, D.K. Kim, C.H. Han, N.M. Hwang, Philos. Mag. Lett., 92 (2012) 344-351.

[80] M. Matsuo, ISIJ Int., 29 (1989) 809-827.

[81] Y. Shimizu, Y. Ito, Y. Iida, Metall. Trans. A, 17 (1986) 1323-1334.

[82] S. Mishra, C. Därmann, K. Lücke, Acta Metall., 32 (1984) 2185-2201.

[83] A. Böttcher, K. Lücke, Acta Metall. Mater., 41 (1993) 2503-2514.

[84] B.J. Duggan, M.Z. Quadir, R. Penelle, in: Mater. Sci. Forum, 2007, pp. 723-728.

[85] C.G. Dunn, Acta Metall., 2 (1954) 173-183.

[86] D. Dorner, S. Zaefferer, D. Raabe, Acta Mater., 55 (2007) 2519-2530.

[87] K. Ushioda, W.B. Hutchinson, ISIJ Int., 29 (1989) 862-867.

[88] T. Haratani, W.B. Hutchinson, I.L. Dillamore, P. Bate, Met. Sci., 18 (1984) 57-65.

[89] D. Dorner, S. Zaefferer, L. Lahn, D. Raabe, J. Magn. Magn. Mater., 304 (2006) 183-186.

[90] H.K. Park, S.J. Kim, H. Nam Han, C.H. Han, N.M. Hwang, Mater. Trans., 51 (2010) 1547-1552.

[91] Y. Ushigami, K. Kawasaki, T. Nakayama, Y. Suga, J. Harase, N. Takahashi, Mater. Sci. Forum, 157-6 (1994) 1081-1086.

[92] Y. Ushigami, Y. Suga, N. Takahashi, K. Kawasaki, Y. Chikaura, H. Kii, J. Mater. Eng., 13 (1991) 113-118.

[93] H.K. Park, S.D. Kim, S.C. Park, J.T. Park, N.M. Hwang, Scripta Mater., 62 (2010) 376-378.

[94] H.K. Park, H.G. Kang, C.S. Park, M.Y. Huh, N.M. Hwang, Metall. Mater. Trans. A, 43 (2012) 5218-5223.

[95] D. Dingley, JMic, 213 (2004) 214-224.

[96] C. Moussa, M. Bernacki, R. Besnard, N. Bozzolo, IOP Conference Series: Materials Science and Engineering, 89 (2015) 012038.

[97] S.I. Wright, M.M. Nowell, D.P. Field, Microsc. Microanal., 17 (2011) 316-329.

[98] B.C. Valek, X-ray Microdiffraction Studies of Mechanical Behavior and Electromigration in Thin Film Structures, Ph. D. Thesis, Stanford University, 2003

[99] A. Budiman, Synchrotron White-Beam X-ray Microdiffraction at the Advanced Light Source, Berkeley Lab, in: Springer (Ed.), Probing Crystal Plasticity at the Nanoscales: Synchrotron X-ray Microdiffraction, Springer 2015, pp. 15-35.

[100] G.E. Ice, R.I. Barabash, White Beam Microdiffraction and Dislocations Gradients, in: F.R.N. Nabarro, J.P. Hirth (Eds.), Dislocations in Solids, Elsevier, 2007, pp. 499-601.

[101] N. Tamura, A.A. MacDowell, R. Spolenak, B.C. Valek, J.C. Bravman, W.L. Brown, R.S. Celestre, H.A. Padmore, B.W. Batterman, J.R. Patel, J. Sychrotron Radiat., 10 (2003) 137-143.

[102] N. Tamura, A. MacDowell, R. Spolenak, B. Valek, J. Bravman, W. Brown, R. Celestre, H. Padmore, B. Batterman, J. Patel, J. Sychrotron Radiat., 10 (2003) 137-143.

[103] J.-S. Chung, G.E. Ice, J. Appl. Phys., 86 (1999) 5249-5255.

[104] R.I. Barabash, G.E. Ice, F.J. Walker, J. Appl. Phys., 93 (2003) 1457-1464.

[105] R.I. Barabash, G.E. Ice, N. Tamura, B.C. Valek, J.C. Bravman, R. Spolenak, J.R. Patel, J. Appl. Phys., 93 (2003) 5701-5706.

[106] R.I. Barabash, G.E. Ice, B.C. Larson, W. Yang, Rev. Sci. Instrum., 73 (2002) 1652-1654.

[107] A.S. Budiman, W.D. Nix, N. Tamura, B.C. Valek, K. Gadre, J. Maiz, R. Spolenak, J.R. Patel, Appl. Phys. Lett., 88 (2006) 233515.

[108] D. Hull, D.J. Bacon, Dislocations in Other Crystal Structures, in: D. Hull, D.J. Bacon (Eds.), Introduction to Dislocations (Fourth Ed.), Butterworth-Heinemann, Oxford, 2001, pp. 102-127.

[109] F.J. Humphreys, M. Hatherly, The Structure and Energy of Grain Boundaries, in: F.J.H. Hatherly (Ed.), Recrystallization and Related Annealing Phenomena (Second Ed.), Elsevier, Oxford, 2004, pp. 91-119.

[110] R. Abbaschian, R.E. Reed-Hill, Physical Metallurgy Principles, Cengage

Learning, 2008.

[111] H.-S. Shim, T.-W. Na, J.-S. Chung, S.-B. Kwon, K. Gil, J.-T. Park, N.-M. Hwang, Scripta Mater., 116 (2016) 71-75.

[112] Y. Wu, X. Zhao, C.-s. He, Z.-p. Zhao, L. Zuo, C. Esling, T. Nonferr. Metal. Soc., 17 (2007) 143-147.

[113] W. Liu, T.K. Wu, A. Godfrey, Q. Liu, Scripta Mater., 52 (2005) 495-499.

[114] Z.C. Hu, C.S. He, X. Zhao, L. Zuo, J. Mater. Sci., 39 (2004) 4231-4234.

[115] C.S. He, Y.D. Zhang, Y.N. Wang, X. Zhao, L. Zuo, C. Esling, Scripta Mater., 48 (2003) 737-742.

[116] K. Jung, H. Conrad, J. Mater. Sci., 39 (2004) 6483-6486.

[117] W. Liu, K.M. Liang, Y.K. Zheng, J.Z. Cui, J. Mater. Sci. Lett., 15 (1996) 1327-1329.

[118] W. Liu, J.Z. Cui, Scripta Metall. Mater., 33 (1995) 623-626.

[119] C.C. Koch, Mater. Sci. Eng. A, 287 (2000) 213-218.

[120] W. Liu, J.Z. Cui, Mater. Res. Bull., 32 (1997) 1411-1417.

[121] Y.D.Z. Z. C. Hu, X. Zhao, L. Zuo, C. Esling, Solid State Phenom., 105 (2005) 169-174.

[122] T.K. Wu, W. Liu, X.L. Li, Q. Liu, Mater. Lett., 59 (2005) 1365-1368.

[123] H.S. Shim, N.M. Hwang, Korean J. Met. Mater., 52 (2014) 663-687.

[124] H.D. Joo, J.T. Park, C.S. Kim, K.S. Han, J.K. Kim, J.W. Seo, J.S. Lim, B.G. Kim, M.S. Kwon, H.J. Choi, in, Google Patents, 2009.

[125] E. Heyn, Metallographist, 5 (1903) 37-64.

[126] D.P. Field, L.T. Bradford, M.M. Nowell, T.M. Lillo, Acta Mater., 55 (2007) 4233-4241.

[127] R.J. McCabe, D.F. Teter, J. Microsc., 223 (2006) 33-39.

[128] H.-R. Jin, S.-H. Yoon, J.-H. Lee, J.-H. Lee, N.M. Hwang, D.-Y. Kim, J.-H. Han, J. Am. Ceram. Soc., 87 (2004) 1747-1752.

[129] A.-D. Li, Y.-J. Wang, S. Huang, J.-B. Cheng, D. Wu, N.-B. Ming, J. Cryst. Growth, 268 (2004) 198-203.

[130] Z.-H. Cao, F. Wang, L. Wang, X.-K. Meng, Phys. Rev. B, 81 (2010) 113405.

[131] Grain-boundary structure and kinetics : papers, in: R.W. Balluffi (Ed.), American Society for Metals, Metals Park, Ohio, 1979.

[132] D.A. Porter, K.E. Easterling, M. Sherif, Phase Transformations in Metals and Alloys, Third Edition (Revised Reprint), CRC Press, 2009.

# 요약(국문초록)

# 금속재료에서의 비정상 입자 성장

비정상 입자 성장 현상은 변형된 금속 재료를 열처리 시 주로 나타나게 된다. 이 비정상 입자성장은 여러 금속 시스템에서 발견이 되는데, 그 중 가장 대표적인 사례는 Fe-3%Si 강에서 Goss 결정립의 선택적 비정상 입자 성장을 하는 것이다. Fe-3%Si 강에서 Goss 결정립의 선택적 비정상 입자 성장 메커니즘에 대하여 수 많은 연구자들의 오랜 시간 노력에도 불구하고, 1933년 Goss의 발견 이후 현재까지 풀리지 않는 문제로 남아있다. 본 연구 그룹에서는 이 현상을 설명하기 위한 노력으로 비정상 입자 성장의 메커니즘을 아결정립계에 의한 고상 젖음 이론으로 설명을 하고 있다. 이 이론에 따르면, 매우 낮은 에너지를 가지고 있는 아결정립계 가 Goss 결정립에만 선택적으로 존재하고, 이 아결정립계가 고상 젖음에 의한 성장 속도를 매우 증가 시킴으로써 비정상 입자성장을 일으키게 된다. 이 논문에서는 이 이론의 타당성을 입증하기 위하여 싱크로트론 X선 미세회절법을 이용하여 비정상 입자성장 초기단계의 Goss 결정립 내부에 실제로 아결정립계가 존재하는지 확인하였다. 싱크로트론 X선 미세회절법을 이용하여 분석한 결과, 아결정립계에 의한 Laue 회절 피크의 갈라짐 현상이 Goss 결정립에서만 관측이 되었고 주변의 matrix 결정

립에서는 관측이 되지 않았다. 즉 싱크로트론 X선 미세회절을 통해 Goss 결정립 내부에서만 아결정립계가 존재한다는 것을 밝혔다. 이 관찰된 아결정립계는 0.6도 미만의 아주 작은 misorientation angle을 가지고 있는 것으로 측정 되었다. Laue 회절 피크의 갈라짐 현상이 일어나는 위치와 방향을 바탕으로 아결정립계의 분포와 아결정립계를 구성하는 전위의 특성 등을 분석하였다.

아결정립계에 의한 고상 젖음 이론과 Goss 결정립에서만 아결정립계가 관측된 실험 결과를 바탕으로, Goss 결정립만 비정상 입자 성장을 일으키는 Fe-3%Si 강에서 Goss와는 전혀 다른 결정 방위를 가진 결정립에 아결정립계를 인위적으로 형성시켜 비정상 입자 성장을 유도하였다. 1차 재결정 완료 시편에 국부적으로 indentation을 가한 후 다시 1차 재결정 열처리를 하여 아결정립계를 형성 시킨 후 2차 재결정 열처리를 한 결과, Goss 결정 방위가 아닌 전혀 다른 결정 방위를 가진 결정립이 비정상 입자 성장을 일으킨 것을 확인하였다. 이러한 사실을 바탕으로 본 연구 그룹에서 주장하는 메커니즘을 통해 비정상 입자성장을 제어할 수 있다는 가능성을 제시하였다.

전기적 전하가 금속의 미세조직에 영향을 주는 새로운 요인이 될 수 있는 가능성을 검토하기 위해, 열처리 중 전기장을 가하였을 때 재결정과 결정립 성장에 미치는 영향을 확인하였다. 순철과 Fe-2.9%Si 합금에서 열처리 중 전기장을 가하였을 때 재결정과 결정립 성장의 속도가 모두 증가한다는 것을 실험적으로 확인하였다. 또한, 비정상 입자성장이 일어나는 Fe-3%Si 강과 Al 5052 합금에서 특징적으로 관찰되는 island 결정

립의 제거 거동이 전기장에 의해 어떻게 변화되는지 확인하였다. 전기장을 가하여 열처리를 한 결과 island 결정립의 제거 속도가 증가하였다. Fe-3%Si 강의 경우 자성을 악영향을 미치는 island 결정립을 제거하기 위해 산업에서는 고온에서 장시간 열처리를 하게 되는데, 전기장을 가함으로써 열처리 시간을 단축 시킬 수 있는 가능성을 제시하였다.

---

**표제어**: 비정상 입자성장; 고상 젖음 이론; 아결정립계; 싱크로트론 X 선 미세회절; 전기장; 재결정; 결정립 성장

**학 번**: 2011-20648